Chapter 3
Design and Implementation of Hardware and Software Systems for EEG-fMRI

In this chapter we describe the design and implementation of a hardware and software system for recording EEG during fMRI. The elements of this system include: 1) An EEG amplification and analog-to-digital conversion system featuring low-noise and high-dyanamic range that is electromagnetically compatible for use within the MRI; 2) A computer hardware and software platform for EEG data acquisition that integrates EEG recordings with external signals such as event triggers and physiological monitoring, with a user-expandable software platform offering the capability to do real-time EEG signal processing; 3) An EEG electrode system that reduces MRI-related noise coupling and radio-frequency (RF) specific absorption rate (SAR) relative to conventional EEG electrodes; 4) A stimulus delivery system integrated with the EEG acquisition system featuring a headphone system for use during MRI offering passive noise protection, high frequency response, and compatibility with ERP recordings. This system is fully compatible with 7 T MRI systems and can also be used for high-speed electrophysiological recordings with minor adjustments to the data acquisition software and the addition of a pre-amplifier buffer system. We describe the design and implementation of each component below.

3.1. An EEG Amplification and Analog-to-Digital Conversion (ADC) System for Use during MRI

In this section we describe an amplification and analog-to-digital conversion system for EEG-fMRI. This system is designed to have *high dynamic range* to prevent saturation from gradient-induced artifacts during MRI, with a *frequency response down to DC* to allow for a fast recovery after MRI image acquisition. *ADC is performed in close proximity to the MRI bore* to limit the loop size of electrode leads and amplifier cables, reducing environmental noise coupling from the static and gradient magnetic fields as well as RF-related increases in SAR.

3.1.1. First Stage Amplification

The first-stage amplification system was built around the Linear Technology LT1167 instrumentation amplifier (Linear Technology Corporation, Milpitas, CA), which possess a number of features particularly appropriate for the EEG-fMRI application. Its low gain nonlinearity (<10ppm), high bandwidth (120 kHz with gain of 100), wide power supply range (V_S = +/-18V) and output range (within 1.3V of V_S), allow for a high dynamic range (Linear Technology Corporation, 1998). Its low input bias current of (<320pA) allows for direct coupling to the source without the use of input bias resistors that reduce input impedance, facilitating the use of higher-impedance EEG electrode systems designed to reduce SAR. The LT1167 is also well-suited to reducing RF and gradient-induced noise coupling with its high common-mode rejection-ratio (CMMR; >120 dB for gain of 100) and power-supply rejection-ratio (PSRR; >131 dB for gain of

100). Its availability in a small-outline integrated circuit package (SOIC; 3.9 X 4.9 mm) is well-suited for a compact PCB layout with small loop sizes to reduce RF and gradient pickup.

The LT1167 was used to provide 32 channels of EEG amplification, with a gain of 50, a power supply of +/-10V, and output coupling resistor of 3.6 kOhm, to provide a 4-kHz first-order low-pass pole when coupled to the 70nF filter capacitors at the input to the ADC unit (to be discussed in Section 3.1.3), as illustrated in Figure 3.1. Traditional AC-coupling capacitors were omitted to provide frequency response down to DC, and DC-coupling bias resistors were omitted to make full use of the amplifier CMMR. The amplifiers were laid out as four 8-channel modules on a double-sided four-layer PCB. The amplifiers received input from EEG electrodes via a custom-made filtered 21-pin micro-D connector, and amplifier outputs were connected to the ADC unit using a double-shielded micro-D cable (to be described below in Section 3.1.3).

3.1.2. Analog-to-Digital Conversion

The analog-to-digital converter unit was designed to operate in close proximity to the MRI bore to reduce RF and gradient noise coupling, with high dynamic range to prevent saturation and allow for removal of MRI-related EEG artifacts. While amplifier circuits possessing high CMRR and PSRR can function properly in the presence of RF and gradient-induced noise, ADC components contain sample-and-hold elements that behave as floating capacitors, rendering them sensitive to fluctuating magnetic fields that cannot be shielded. To balance the trade-off between low noise coupling from EEG/amplifier leads and ADC sensitivity to the gradients, we designed the ADC unit to

operate just outside the MRI bore, connecting it to the amplifier system with a long shielded cable as described above. Communication and data transmission with external computers was accomplished by way of digital optical communications, for both the actual EEG data and the scan clock used to sample the data. This scan clock ("SYNC") was used to synchronize EEG acquisition with external signals such as event triggers or physiological data. The ADC process is controlled by a digital signal processing (DSP) microcontroller, which manages the ADC timing and data transfer to the optical communications hardware. These elements are illustrated in Figure 3.2.

To achieve high dynamic range, we selected the Burr-Brown ADS1254 ADC, a low-power, low-noise, high-speed ADC with 24-bit resolution (Burr-Brown, a division of Texas instruments, Dallas, TX). Each ADS1254 chip has four differential inputs, which can be multiplexed at a rate of up to 1 kHz per channel when operated with a system clock rate of 8 MHz (Burr-Brown Products, 2001). Alternatively, a single channel can be sampled at up to 20 kHz. To provide 32 channels of EEG, an architecture using 8 ADS1254's was chosen, each running with 4-channel multiplexing at 1 kHz. If higher-rate sampling were required, a single channel from each ADS1254 could be sampled, giving 8 channels at 20 kHz per channel. The ADS1254 chips were controlled by an SX48 DSP unit (Ubicom, Inc., Mountain View, CA) running at 48 MHz. To reduce RF noise coupling to the analog input stages of the ADC system, clock timing was provided by a single 48 MHz clock driving a programmable divide-by-six counter (DS1075; Dallas Semiconductor, a subsidiary of Maxim Integrated Products, Dallas, TX), which provided the 8 MHz clock for the ADS1254. The analog input to each ADS1254 unit was first anti-alias filtered and then re-scaled to a 0-to-5V reference range using an op-amp-based

scaling and level-shift circuit recommended in the ADS1254 datasheet (Burr-Brown Products, 2001). Low-pass anti-aliasing filtration was provided by a one-pole RC divider whose capacitance was user-selectable via a transistor switch system controlled by the SX64 to provide a cutoff frequency of either 12 or 24 kHz. Two forms of optical communication are provided by the system. The first is a universal serial bus (USB) optical link that is used to control the acquisition device and to transmit the sampled EEG data. This is provided by the combination of a USB interface module (DLP-USB245M; DLP Design, Allen, TX) integrated into the ADC system circuit, which is then connected to an optical USB extension cable (Opticis M2-100; Opticis North America Ltd., Richmond Hill, Ontario, Canada). The second is a high-speed optical line (Agilent HFBR-1521; Agilent Technologies, Palo Alto, CA) that is driven by the channel selection portion of the SX48 processor, providing one clock pulse for every 8 channels sampled (4 kHz in 32 channel mode, 20 kHz in 8 channel mode), providing a synchronization (SYNC) signal for external signals such as event triggers and physiological recordings with the EEG. A block-diagram for these system components is provided in Figure 3.3.

The PCB layout for the ADC unit is divided into three isolation zones organized according to power requirements and noise sensitivity (Figure 3.4): 1) A 5V digital zone supporting the SX64, USB, Versatile Link, and digital clock modules; 2) A 3.3V digital zone supporting the ADS1254 ADC chips; and 3) A 5V analog zone supporting the scaling and level-shift modules, and supplying +/-10V power for the amplifier system. Power was provided by a pair of 18A-h 12-V lead acid batteries (TR18-12; Tempest Battery Manufacturing Company, Ltd., Campbell, CA) connected in series and center-tapped to provide +12V, GND (center tap), and -12V terminals. A pair of Schottky

diodes were used to provide accidental reverse battery protection (International Rectifier 20L15TS, International Rectifier, El Segundo, CA). PCB layout, DSP programming, DLP interface programming, and board population were performed by TechEn, Inc. (Milton, MA).

3.1.3. Shielding and Grounding for Electromagnetic Compatibility

A shielding and grounding system was constructed to achieve electromagnetic compatibility for MRI. The primary objectives were to: 1) Design and construct chassis elements to provide circumferential contact and conductivity at all chassis seams or interconnects, in order to minimize slot radiators; 2) Use filtered interconnects to provide RF attenuation for all input-output lines; and 3) Make multiple low-impedance connections between the chassis and circuit "grounds," in order to provide low impedance return paths for RF currents radiated from digital components or PCB traces.

Plastic enclosures were chosen for the amplifier and ADC units to fit the required PCB and external connector dimensions (Pactec LH-64-130 for amplifier unit, CM-69-240 for ADC unit; Pactec, Inc., Concordville, PA). The internal surfaces of the enclosures were coated with aluminum using a vacuum deposition technique giving a coating thickness of approximately 100 microns (Vacuum Technologies Inc., Reedsburg, WI), with care taken to coat the interlocking flanges of each chassis piece to ensure electrical contact. An important mechanical feature of these enclosure models was the use of flat "endplates" for input-output connector attachment (Figure 3.5). The supplied plastic endplates were replaced with custom-made endplates designed to improve electrical contact with the rest of the chassis shell, and to provide precise circumferential

contact with input-output connectors. Construction details for these custom-made endplates are provided in **Appendix 3A.1.** The ADC unit's digital ground was connected to the chassis at the battery input terminal, while its analog ground was connected near the EEG input-output lines and the +/-10V regulators (Figure 3A.1.c). The shielded chassis for the amplifier unit was constructed using materials and methods identical to those used for the ADC unit, but with a different filtered interconnect system. In particular, each 8-channel amplifier module was coupled to EEG electrodes using hand-made 21-pin filtered micro-D connectors featuring 1nF capacitor arrays. The amplifier analog ground was terminated to the amplifier chassis at each of the filter-connector's ground pins. Construction details for the micro-D filtered connector are provided in **Appendix 3A.1**.

The 32-EEG channel outputs were connected to the ADC unit using a non-ferromagnetic 9-foot 37-pin micro-D double-shielded cable featuring circumferentially-conductive backshells and circumferential termination to cable shields (Glenair 177-225; Glenair, Glendale, CA). At 9-feet, this cable is long enough to reach from the head coil to the bore edge in most MRI systems, including the Siemens Allegra 3T, Siemens Trio 3T, and Siemens Magnetom 7T. Like the ADC unit, connector holes in the conductive panels of the amplifier chassis were precision cut using the T-Tech QuickCircuit-7000 (T-Tech, Norcross, GA) to provide circumferential contact and conductivity for each connector. Cable-to-chassis connections were made robust by using jackpost and screw connections. In practice, DC impedance from the EEG connector shell to the ADC battery GND terminal was approximately 0.2 to 0.3 ohms when measured with a standard voltmeter.

3.1.4. System Performance

The LT1167-based amplifier system described above, with its gain of 50, its +/-10V power supply, and its output range of –VS+1.2 to VS-1.3 V, provides a dynamic range of -176 to +174 mV. The ADS1245 provides a 19-bit RMS effective resolution due to inherent noise within the integrated circuit, offering an effective resolution of 0.76uV in the least significant bit (LSB), given an amplifier gain of 50 and an amplifier output range of +/-10V. Typical traces are shown in both time and frequency domain, recorded in a shielded room with a 10Hz, ~10uV input signal provided by a function generator (Figure 3.6.a) and under quiescent conditions with all amplifier channels shorted to ground (Figure 3.6.b). The RMS noise calculated from the quiescent recordings was approximately 0.1517 uV/$Hz^{1/2}$ (bandwidth from 0 to 475 Hz, averaged across all channels). The recovery speed of the amplifier system during MRI is evident from Figure 3.7, which compares a traditional AC-coupled high-gain amplification system (Ives et al., 1993;Mirsattari et al., 2005) during EPI with the present system. Figure 3.8 illustrates the effectiveness of the shielded enclosure system. During one recording session, the cover to the ADC chassis was removed during imaging (middle column of Figure 3.8), resulting in poor image quality compared to images without EEG (left column of Figure 3.8). In a separate imaging session, with the shielding system in place, image noise levels are at nominal levels (right column of Figure 3.8.b).

3.2. Data Acquisition, External Signal Integration, and Real-Time Signal Processing

In this section we describe a computer hardware and software system for EEG acquisition, integration with external signals, graphical display, and real-time signal processing.

3.2.1 Acquisition and Integration of EEG with External Signals

In many EEG-fMRI applications, acquisition of external signals time-locked to the EEG signal is required. For instance, ERP studies require event triggers to mark when different stimuli are presented, while drug studies may require simultaneous physiological monitoring. We have devised a laptop-based data acquisition and integration architecture that draws EEG data from the USB interface, and either digital or analog external signals from the PCMCIA bus, time-locked to the USB interface by way of the SYNC signal discussed in Section 3.1.2 (Figure 3.9). The USB EEG interface is based on the FTDI FT245BM chipset used in the DLP USB module (Future Technology Devices International, Ltd., Glasgow, Scotland, UK; DLP Design, Inc., Allen, TX). A National Instruments DAQCard 6533 high-speed 32-bit parallel digital I/O interface card is used for digital external signals such as event triggers, while a National Instruments DAQCard 6024E high-speed 12-bit analog acquisition card is used for analog acquisitions such as physiological monitoring (National Instruments, Austin, TX). Digital trigger information can be recorded on the 6024E interface by supplying individual trigger lines to one or more of the analog inputs. Acquisition of the external signals is clocked by the EEG-fMRI ADC unit's optical SYNC line through an Agilent Versatile Link receiver (Agilent HFBR-2521, Agilent, Palo Alto, CA). A detailed description of interconnects required for both setups is provided in **Appendix 3A.2**.

3.2.2. Data acquisition software for display, recording, and real-time signal processing

The National Instruments (NI) LabView software development platform (National Instruments, Austin, TX), running within the Microsoft Windows 2000 operating system (Microsoft, Richmond, WA), was used to develop the data acquisition (DAQ) software for this application. LabView is a high-level graphical programming language featuring a wide assortment of built-in data-acquisition, hardware interface, data display, and data analysis functions to speed software development. The LabView development environment offers seamless integration with DAQ devices, either with built-in interfaces for National Instruments data acquisition cards, or with user-programmed DLL's to interface with custom or 3rd party devices. Its modular graphical development system allows for rapid revision and inclusion of new functions, reducing software development cycles. DAQ programs are constructed as "virtual instruments" (VIs) controlled through an intuitive push-button graphical user interface, making the programs easily accessible to a wide range of end-users. Even with these graphical and hardware-integration conveniences, its features are sufficiently rich to retain the control, modularity, flexibility, and processing speed of traditional text-based languages.

DAQ applications in LabView can be constructed using a variety of interface functions spanning a range from high-level functions offering immediate implementation but minimal control, to low-level functions offering a high degree of control but greater development complexity. The data integration architecture described in Section 3.2.1 calls for two buffered data acquisition to run simultaneously: One buffered acquisition process for either the DAQCard 6533 or 6024E, and another for the USB-based EEG

ADC unit. In LabView Versions 6i through 7.1, buffered data acquisitions can be handled through a combination of built-in intermediate-level DAQ functions to configure, start, read, and clear the acquisition, arranged within a while-loop structure (Bishop, 2001). These intermediate-level DAQ functions offer control over acquisition timing, data size, trigger sources, and buffer sizes, among other details, but can be implemented easily within a single VI. Figure 3.10 illustrates simple digital and analog buffered acquisitions using these intermediate-level DAQ functions. Table 3.1 provides an overview of each of these intermediate-level DAQ functions. To integrate the USB EEG acquisition within this control structure, the USB DAQ commands were interfaced with LabView according to this intermediate-level VI formalism. In this way, the USB EEG acquisition could be run in parallel with the digital or analog acquisition using the same while-loop control structure. **Appendix 3A.3** contains a detailed discussion of each of these USB EEG acquisition VI's and their underlying USB DLL commands.

Table 3.1. Overview of Intermediate-Level DAQ Functions for Digital, Analog, and USB EEG acquisitions.

Function Name	Description and Features
NI Intermediate-Level Digital DAQ	
DIO Config	Set Buffer size, device number, port list, group direction (input, output, or both), handshaking parameters
DIO Start	Set number of scans to acquire or continuous, clock/handshake source, clock frequency
DIO Read	Buffered acquisition, tracking scan backlog, providing data output for display, file writing, and analysis
DIO Clear	Terminates acquisition
NI Intermediate-Level Analog DAQ	
AI Config	Sets channel timing, number of channels, input coupling info, input limits, device number, channels, buffer size, group number, number of buffers
AI Start	Sets trigger type, edge or slope trigger, pretrigger scans, number of

	scans to acquire or continuous, scan rate, scan clock source, analog trigger settings
AI Read	Buffered acquisition, tracking scan backlog, providing data output in multiple formats for display, file writing, and analysis
AI Clear	Terminates acquisition
USB EEG Interface	
AI Config 24Bits	Sets multiplexing mode (8 channels or 32 channels), channel number, anti-aliasing filter setting (12 or 24 kHz), and memory location in SX48 for storing configuration ("bank" number, similar in concept to "Process ID")
AI Start 24Bits	Sets configuration "bank," number of scans to acquire or continuous
AI Read 24Bits	Buffered acquisition, reads FIFO when data are present, data output converted to 4(time) x 32(channel) matrix in signed 32-bit integer (I32) for display, file writing, and analysis.
AI Clear 24Bits	Terminates acquisition

Figure 3.11 shows the top-level block diagram of the EEG data acquisition VI. When end-user begins acquisition, temporary files and acquisition processes are configured and started for three separate data streams: 1) The USB EEG data, 2) The DAQCard process for recording external signals (code for the DAQCard 6533 is shown, but is similar for the 6024E) and 3) A keyboard-polling process to record real-time end-user annotations (e.g., "m" for subject movement, "o" for eyes open, "c" for eyes closed, etc.). The initialization process for these acquisitions is described in Figure 3.12. After initialization, all three processes run continuously within a "while-loop" structure, where data are read, displayed, and streamed to disk. Real-time processing modules, such as the low-pass filter module illustrated in Figure 3.10) can also be added within the while-loop structure. At the end of the acquisition, all files are closed and acquisition processes are cleared.

The EEG acquisition front panel is shown in Figure 3.13. The acquisition is started by pressing the "run button" in the upper left corner of the LabView window. The

acquisition will start immediately, and the user can switch between four different 8-channel displays, and can examine the trigger display to ensure that stimulus triggers or external signals are being received properly. Amplitude scaling can be adjusted by using the up- or down-arrow keys, with the blue vertical bar indicating the scale for 100 uV, while time scaling can be adjusted using the left- or right-arrow keys, with the blue horizontal bar showing the scale for one second. Channel legends are displayed on the right-hand side of the front panel. At the end of the experiment, the acquisition is stopped by pressing the "STOP" button. At this point, a file-saving dialog box is displayed prompting the user to provide a filename. The temporary files created at the beginning of the acquisition are then re-named accordingly. The application software, USB interface, and external acquisition DAQCards are run on a Dell Latitude 810C with a 1.7GHz Pentium IV processor, 400 MHz bus, 1 GB of RAM, and 80 GB hard disk. For digital external signals using the DAQCard 6533, assuming a 16-bit digital input running at the base SYNC rate of 4 kHz, approximately 8 MB of disk space are required per minute of recording. Analog external signals using the DAQCard 6024E, assuming 8-channels of external signals at 16-bits, requires approximately 11.5 MB of disk space per minute of recording. Figure 3.14 shows the complete system setup with amplifiers, EEG ADC acquisition unit, external signal card and cable assembly, and acquisition computer.

3.3. Electrode and Motion Sensor Systems for EEG-fMRI

As discussed in Chapter 2, heating due to increases in RF specific absorption rate from placement of scalp EEG electrodes is a potential problem for EEG-fMRI studies. The de-facto standard to prevent electrode heating has been to place discrete resistors, 10

kOhm or larger, at the tip of each electrode (Lemieux et al., 1997), but simple direct calculations (Chapter 2) and RF simulations using realistic head models (Angelone and Bonmassar, 2004) illustrate that these resistors provide little or no power attenuation at the RF frequencies used for MRI, particularly at 3 or 7 Tesla. Modest resistances of as little as 4.2 Ohms/inch (166 Ohms/meter) distributed along the lead, achievable in practice using carbon fiber wires, can bring the SAR close to nominal levels (Angelone and Bonmassar, 2004). Another problem associated with EEG electrodes used during MRI is that motion or vibration within the static field will inductively couple noise signals through loops within the recording circuit. Since head motion, physiological pulsation, and vibration of the head and body are the largest source of this noise, loops formed from the EEG electrode leads provide the greatest opportunity for noise coupling.

We have designed a series of EEG electrodes to provide both RF protection and static field-induced noise attenuation. This system has been constructed from off-the-shelf components in two bipolar montage configurations, one spanning 8 channels along a coronal plane for auditory evoked potential (AEP) measurements, and a 19-electrode 10/20 montage designed for anesthesia and sleep studies (Figure 3.15). Since safety studies and experience at 3 or 7 Tesla had not been well-established at the time of design, the number of electrodes was chosen conservatively to limit RF heating risk. Carbon fiber wires ("Fiber-Ohm;" Marktek, Inc., Chesterfield, MO), with 7 Ohms/inch resistance (276 Ohms/meter), were used to limit increases in SAR, and were connected to Ag/Ag-Cl electrode bodies using conductive epoxy (Circuit Works CW2400, Chemtronics, Kennesaw, GA). These electrode bodies featured plastic housings to prevent direct electrode skin contact (Gereonics, Inc., Solana Beach, CA). To provide a reference

signal for artifact removal using adaptive noise cancellation, a set of motion sensors were constructed from Murata PKM11-4A0 piezo-electric buzzers (Murata Electronics North America, Inc., Smyrna, GA) using similar methods, replacing soldered metallic leads with conductive epoxied carbon fiber leads (Figure 3.16).

To reduce motion-induced inductive noise coupling, the carbon fiber electrode wires were arranged in a "ribbon cable" fashion, with wire lengths cut to fit the appropriate electrode locations for average- to large-sized heads (Figure 3.17). The ribbon cable arrangement reduces motion-induced noise coupling by both reducing loop sizes between differential electrode pairs, and between electrodes and reference, and by holding these leads in a fixed relative position, which allows some of the noise coupling to be eliminated through common-mode rejection (Figure 3.18). The wires were bound together using silicone adhesive sealant, which served both to hold the wires together, and as a mass and damping material to reduce mechanical vibration. Construction details for these electrodes are provided in **Appendix 3A.4**. For complex montage arrangements such as the 10/20 system, the ribbon cable is more practical than twisted pair arrangements reported by some investigators (Goldman et al., 2000), and is likely to offer similar if not better performance due to the practical difficulty of braiding identically-sized loops from individual wires. Electrodes from the coronal montage can be held in place with the combination of EEG paste, tape, and elastic surgical netting, while the 10/20 montage is best held in place with collodion glue and elastic surgical netting.

Increased RF attenuation can be achieved with higher resistance levels, but there are practical limits on the resistance levels available with carbon fiber wires. Commercially available off-the-shelf wires come in two resistance ranges: a low resistance range of 4

to 7 Ohms/inch, and a higher resistance level of 3 M-Ohms/inch and beyond (Personal communication, Art Henn, Marktek, Inc., 2003). RF-attenuating EEG-fMRI electrodes would likely require resistances in the 1 kOhm/inch range at most.[1] Carbon fiber composite wires, blending high and low resistance fibers, could be used to obtain intermediate values in this range, but could be expensive to manufacture in the small quantities required for EEG electrodes (Personal communication, Art Henn, Marktek, Inc., 2003). We have developed an alternative strategy using carbon or silver conductive inks to print or silkscreen electrode wires onto flex-circuit material. With this strategy, it is possible to selectively tune the impedance for each electrode lead, by controlling the mixture of inks used in the electrode, and to precisely layout leads into ribbons to reduce motion-induced noise coupling. A prototype EEG cap using this conductive ink technology with integrated motion sensors has been constructed and is being developed for routine use in EEG-fMRI studies (Vasios et al., 2005) (Figure 3.19), particularly those at high field where RF safety is a major concern.

3.4. An Auditory Stimulus Delivery System for EEG-fMRI

Auditory stimulus presentation during fMRI or EEG-fMRI requires careful consideration of numerous design features, including timing precision, audio fidelity, MRI compatibility, and EEG compatibility. The inherent difficulty in meeting all these design challenges simultaneously is apparent when one examines the EEG-fMRI literature: Numerous groups have been successful at recording visual evoked potentials (VEPs) during fMRI (Bonmassar et al., 1999;Vanni et al., 2004;Garreffa et al., 2004),

[1] EEG leads from our applications have measured anywhere from 16 to 22 inches in length, and with 1 kOhm/inch resistance, this would give total electrode resistances in the range of 16 to 22 kOhm, resulting in a low-pass cutoff of 62 or 45 Hz, respectively, assuming a 1 nF parallel capacitance at input.

while relatively few have been able to record auditory evoked potentials (AEPs) during fMRI., achieving success mainly with simple tone stimuli at long inter-stimulus intervals (Liebenthal et al., 2003). Event-related potential (ERP) studies, regardless of the stimulus modality, require high-precision timing. Timing accuracy can be quantified in terms of average delay (or latency), which refers to the average time difference between the stimulus trigger onset and the actual stimulus onset, and the jitter about that average delay (Figure 3.20). Stimulus delays can be accounted for in ERP analysis simply by introducing an opposite delay prior to averaging, but large jitter values can compromise the ability to discern peaks within the ERP waveform. Audio fidelity, considered broadly, comprises many elements, including the frequency response of the headphone and amplification system, their total harmonic distortion, the maximum volume or loudness achievable by the system, and the degree of background noise, such as the notorious 60-Hz ground loop "hum." Compatibility with the MRI environment requires electromagnetic compatibility, study subject protection from acoustic scanner noise, use of non-ferrous headphone elements, and portability to accommodate multi-user MRI facilities or use in multiple imaging facilities. Audio systems must also be compatible with ERP studies: Auditory ERPs are best observed using stimuli with high bandwidth, such as click trains or noise bursts, and are typically presented using headphones whose frequency response extends to 15 or 20 kHz. Headphones for ERP studies must not introduce stimulus-related noise coupling into the EEG recordings, as this could confound ERP analysis, depending on the experimental paradigm.

Auditory presentation systems fulfilling all these requirements are not available commercially. The requirement to use only non-ferrous components rules out standard

magnetic-coil headphones. Headphones using air-tube sound transmission with sound-attenuating earmuffs (e.g., Avotec SS-3100, Avotec, Inc., Stuart, FL, USA) are popular for fMRI studies, but provide a frequency response of only 4.5 kHz, inadequate for stimuli such as click-trains or noise-bursts that require a high frequency-response. Electrostatic headphones provide a frequency response in excess of 20 kHz, but commercially available models (e.g., Koss ESP-900, Koss Corp., Milwaukee, WI, USA) offer no hearing protection. In addition, as will be shown below, electrostatic headphones emit electromagnetic fields that couple to EEG recordings with an amplitude that is orders of magnitude higher than the EEG signal itself. In the next two sections, we describe a portable, electrically-isolated auditory stimulus presentation system capable of achieving sub-millisecond timing precision, combined with an electrostatic MRI-compatible headphone system with passive sound-attenuation and electrical shielding that eliminates noise coupling with EEG.

3.4.1. Stimulus presentation

Stimuli were delivered using an IBM Thinkpad T40 laptop (1.6 GHz P4, 512MB 266 MHz RAM, 80GB 4500rpm hard drive; IBM, White Plains, NY) running Microsoft Windows XP (Microsoft Corporation, Redmond, WA). To boost sound output levels and signal to noise relative to the onboard sound card, an Echo Indigo Digital Audio PCMCIA card (Echo Digital Audio Corp., Carpinteria, CA) was used as the sound device. The stimulus presentation laptop was configured to deliver stimulus triggers through its parallel port and was connected to the EEG acquisition computer as described in Section 3.2 and Appendix 3A.2. Task-related button-press responses were recorded

using a USB button box configured as a keyboard device to send the numbers "1" through "4" for each of the keypad buttons. With the headphone system (described below), stimulus delivery and EEG acquisition computers connected and AC powered with no stimulus, there was no audible background noise of any kind. When the USB button box was added to this configuration, a faint 60-Hz hum could be perceived. This background hum was eliminated by electrically isolating the USB button box from the rest of the system using an Opticis M2-100 optical USB extension cable (Opticis North America Ltd., Richmond Hill, Ontario, Canada). Stimuli were scripted and delivered using NeuroBehavioral Systems Presentation 0.76 (NeuroBehavioral Systems, Albany, CA). Stimulus delay and jitter relative to recorded parallel port stimulus triggers were measured by recording stimuli and triggers under different hardware and scripting arrangements. Depending on the laptop and sound hardware used, the average delay could be brought to within 1 msec, with a jitter of less than 1 msec, sufficiently accurate for most ERP experiments. A detailed description of the testing protocol and results for different laptop, software, and audio hardware configurations is provided in **Appendix 3A.5**.

3.4.2. A high-fidelity headphone system for simultaneous EEG-fMRI studies

A set of headphones were constructed for EEG-fMRI studies, featuring the high-fidelity audio performance of electrostatic headphones, passive sound attenuation, and electrical shielding for compatibility with EEG and ERP studies. The electrostatic headphone elements were removed from a set of Koss ESP-950 headphones (Koss Corp., Milwaukee, WI), electrically shielded, and placed within a set of sound-attenuating

earmuffs (Silenta Ergomax, Oy Silenta Ltd., Finland). Electrical shielding was accomplished by replacing the first 6 feet of headphone cable with double-shielded (braid over foil) computer cabling, and by enclosing each headphone element within a conductive fabric sock constructed from silver-coated sheer nylon mesh (Less EMF Cat. #A209, Less EMF Inc., Albany, NY). The conductive fabric mesh was chosen for its low resistivity (<5 Ohms/square) and because of its thin, light, porous structure, providing minimal absorption of acoustic energy. Shielded cabling was limited to 6 feet to reduce capacitive load on the electrostatic amplifier system (<600 pF). The cable shield was connected to the conductive sock using copper foil tape, and terminated on a copper mesh housing encasing the Koss amplifier unit via a single wire running along the remaining length of the headphone cable. The conductive sock was electrically insulated from the headphone using a thin plastic membrane. The amplifier unit was powered from a 9.6V rechargeable battery placed outside the MRI room and routed through the penetration panel. Battery power was chosen over AC power to reduce the risk of electrical shock in the event that bodily fluids such as mucosal secretions or vomitus cause a short circuit within the headphone elements. The battery ground terminal and amplifier shield were connected at the penetration panel. Construction details for the headphone system are provided in **Appendix 3A.6**.

Acoustic attenuation recordings were made using an electret condenser mic (Shure SM-93, Shure, Niles, IL) by comparing scanner noise during gradient echo functional scanning (Siemens Trio) with the microphone placed inside and then directly outside the headphone earmuff, with the headphones in place on a human volunteer. Acoustic attenuation measurements were made for the electrostatic system as well as an

off-the-shelf Avotec MRI-compatible audio system (Avotec SS-3100, Avotec, Inc., Stuart, FL). Electromagnetic noise coupling measurements were made by coating an MRI phantom in EEG paste (Elefix, Nihon Kohden, Japan), placing adjacent bipolar pairs of EEG electrodes in the coronal plane to simulate the M1/2, T7/8, C3/4, C1/2, and Cz positions, fixing the headphone earpieces over the phantom while presenting sound stimuli, and recording using the EEG/fMRI recording system described earlier. Sound stimuli consisted of noise-bursts (12.5 msec) and click-trains (1 msec) sampled at 44.1 kHz, presented at 25 msec intervals, 30 seconds ON, 30 seconds OFF, using the stimulus presentation system described in Section 3.4.1. Recordings were made with the headphone shield disconnected and floating ("unshielded") and then with the shield connected ("shielded"). Auditory ERPs and ASSRs were recorded from 24 human volunteers (similar stimuli and EEG setup) using the shielded-electrostatic headphone system. All studies were conducted with the approval of the Human Studies Committee at the Massachusetts General Hospital (Boston, MA), with informed consent from all volunteers.

Attenuation and noise coupling were studied by computing multi-taper power spectral estimates (Percival and Walden, 1993) for each condition, and taking ratios of the appropriate power spectra to determine attenuation or noise coupling. To quantify acoustic attenuation $A(e^{j\omega})$, the ratio of power spectra for sound recordings with microphones inside the earmuffs ($P_{inside}(e^{j\omega})$), were compared to the power spectra for recordings with microphones outside the earmuffs ($P_{outside}(e^{j\omega})$):

$$A(e^{j\omega}) = \frac{P_{inside}(e^{j\omega})}{P_{outside}(e^{j\omega})}. \qquad (0.1)$$

To quantify electromagnetic noise coupling $C(e^{j\omega})$ for each shielding condition ("unshielded" or "shielded"), the EEG power spectra with stimulus "ON" ($P_{EEG,ON}(e^{j\omega})$) was compared to that for with the stimulus "OFF" ($P_{EEG,OFF}(e^{j\omega})$):

$$C(e^{j\omega}) = \frac{P_{EEG,ON}(e^{j\omega})}{P_{EEG,OFF}(e^{j\omega})}. \tag{0.2}$$

Acoustic attenuation for the shielded-electrostatic and Avotec systems were similar, 32.8 and 38.1 dB, respectively, averaged between 0.8 and 20 kHz. Figure 3.21 shows electromagnetic noise coupling $C(e^{j\omega})$ on a dB scale for the unshielded (solid) and shielded (dotted) cases, illustrating that the shielding reduces electromagnetic noise coupling by over 40dB throughout the bandwidth of the EEG recording device. To quantify the shielding effectiveness with greater sensitivity, Figure 3.22 compares the shielded noise coupling (Phantom) with the 40-Hz ASSR from a human volunteer on a linear scale (perfect shielding corresponds to $C(e^{j\omega}) = 1$), illustrating that the shielded noise coupling is indistinguishable from background noise and is well below the level of the measured electrophysiological response (approx 1 uV p-p). For the human studies, there were no discernable image artifacts during MRI due to the headphones.

3.5. Summary

In this chapter we have described the design and implementation of a hardware and software system for recording EEG during fMRI consisting of: 1) An EEG amplification and analog-to-digital conversion system featuring low-noise and high-dyanamic range that is electromagnetically compatible for use within the MRI; 2) A

computer hardware and software platform for EEG data acquisition that integrates EEG recordings with external signals such as event triggers and physiological monitoring, with a user-expandable software platform offering the capability to do real-time EEG signal processing; 3) An EEG electrode system that reduces MRI-related noise coupling and radio-frequency (RF) specific absorption rate (SAR) relative to conventional EEG electrodes; 4) A stimulus delivery system integrated with the EEG acquisition system featuring a headphone system for use during MRI offering passive noise protection, high frequency response, and compatibility with ERP recordings.

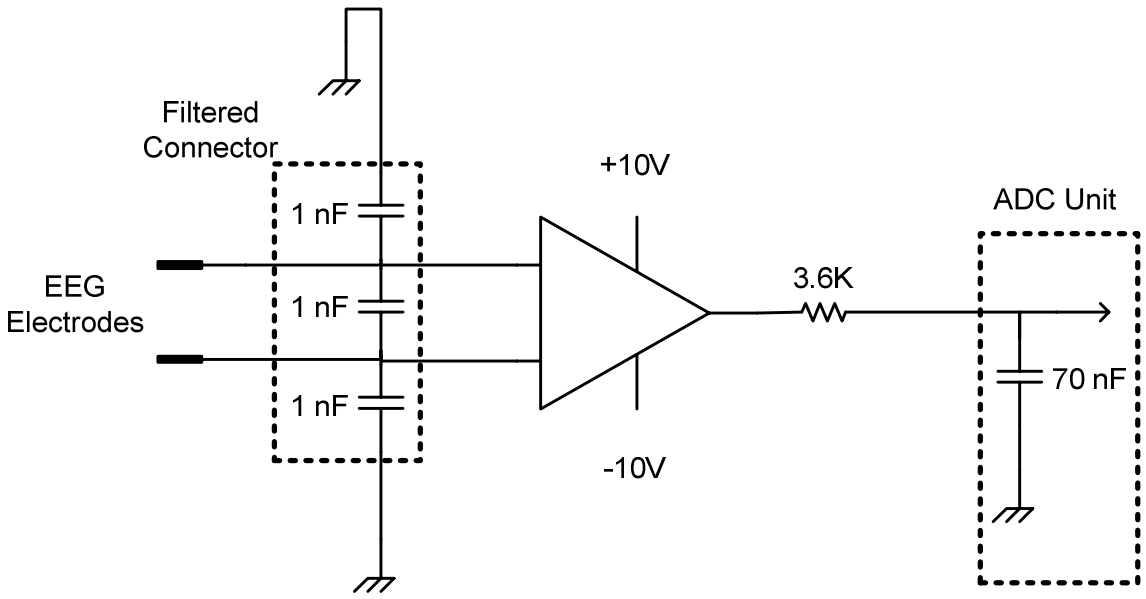

Figure 3.1. First-stage amplifier circuit, illustrating input filtered capacitor array, chassis connections, and output resistor interaction with feed-through capacitor in ADC unit.

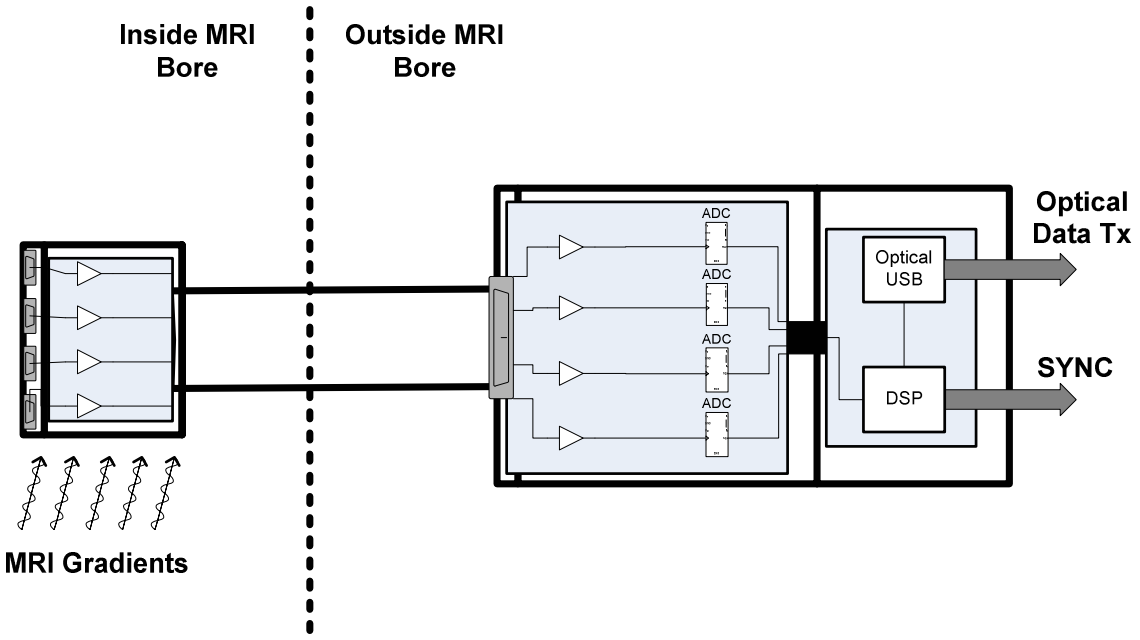

Figure 3.2. Layout of amplifier and ADC units relative to MRI bore. The amplifier is located within the bore, close to the head coil, to minimize inductive noise coupling through electrode lead wires. The ADC unit is located farther from the MRI bore to reduce the influence of the gradients on its more sensitive sample-and-hold elements.

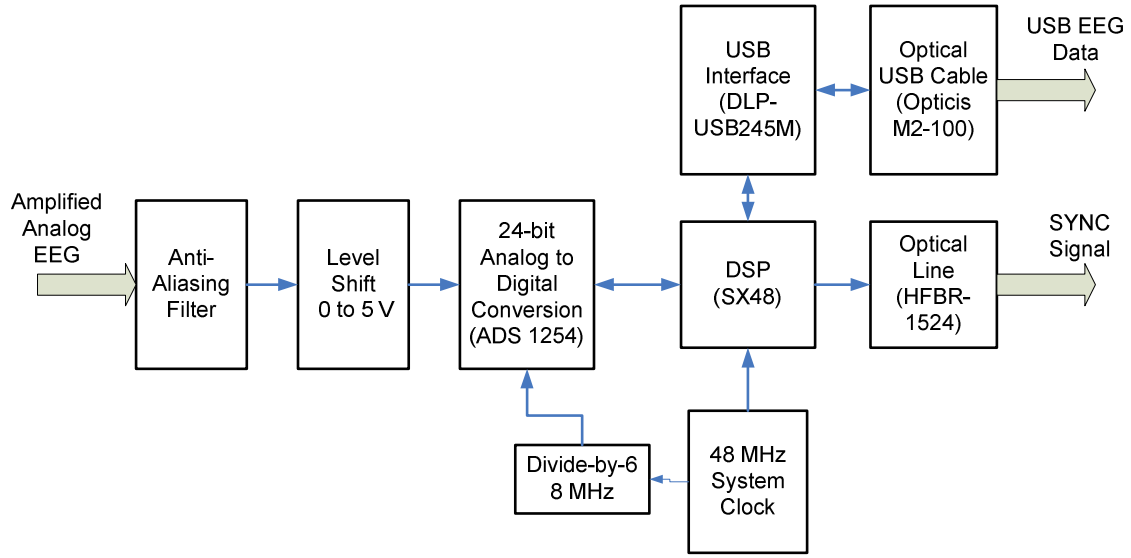

Figure 3.3. Detailed block diagram of ADC system components.

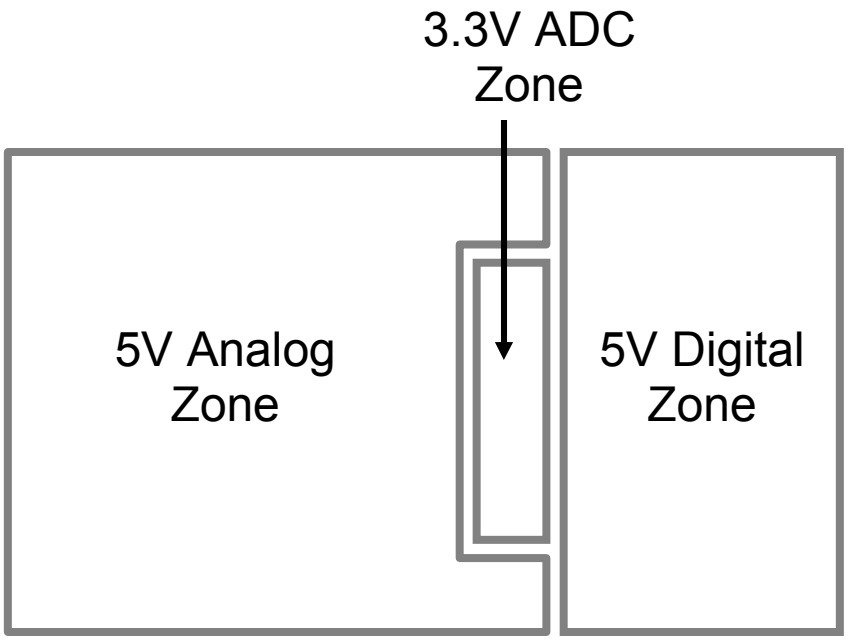

Figure 3.4. Isolation zones for PCB layout of ADC unit.

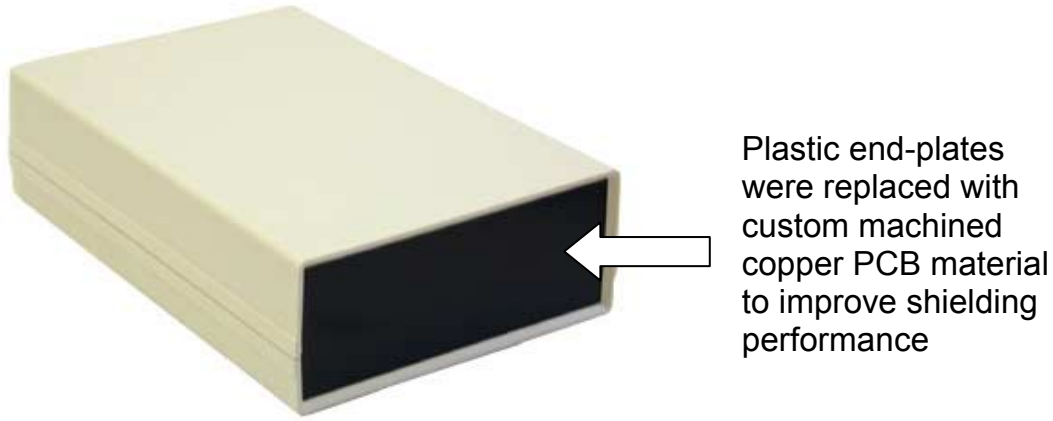

Figure 3.5. Plastic chassis for ADC unit, illustrating chassis end-plates that were replaced with precision-cut copper-clad plates described in Appendix 3A.1. The internal surfaces of both chassis were vacuum deposited with 100 micron aluminum (Vacuum Technologies Incorporated, Reedsburg, WI), with care taken to coat all interlocking surfaces to ensure good contact and eliminate slot radiators. The amplifier chassis was constructed using similar materials and methods.

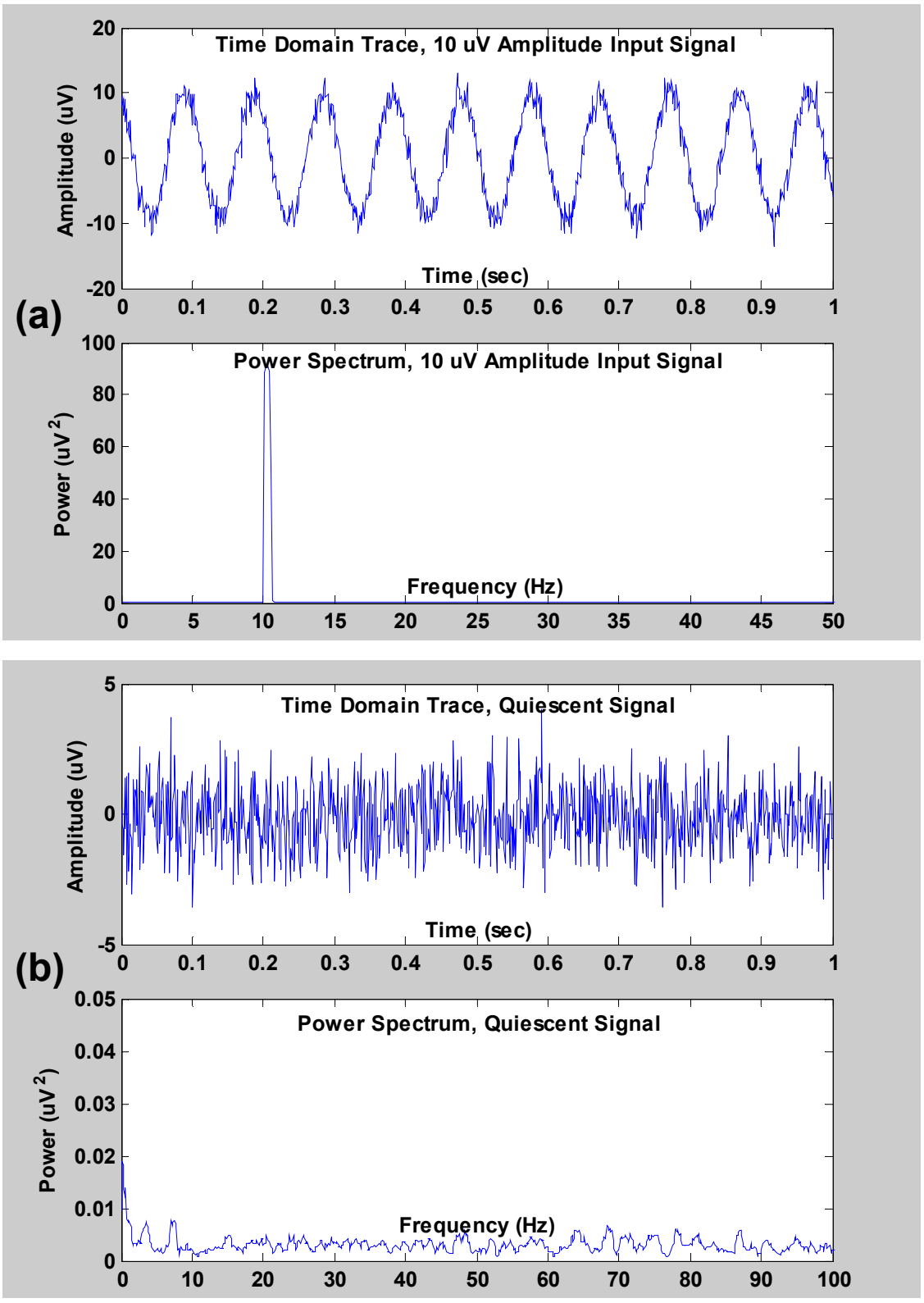

Figure 3.6. Typical recording traces for EEG-fMRI amplification and ADC units: (a) Driven by function generator with 10Hz, ~10uV signal; (b) Quiescent signals with input grounded.

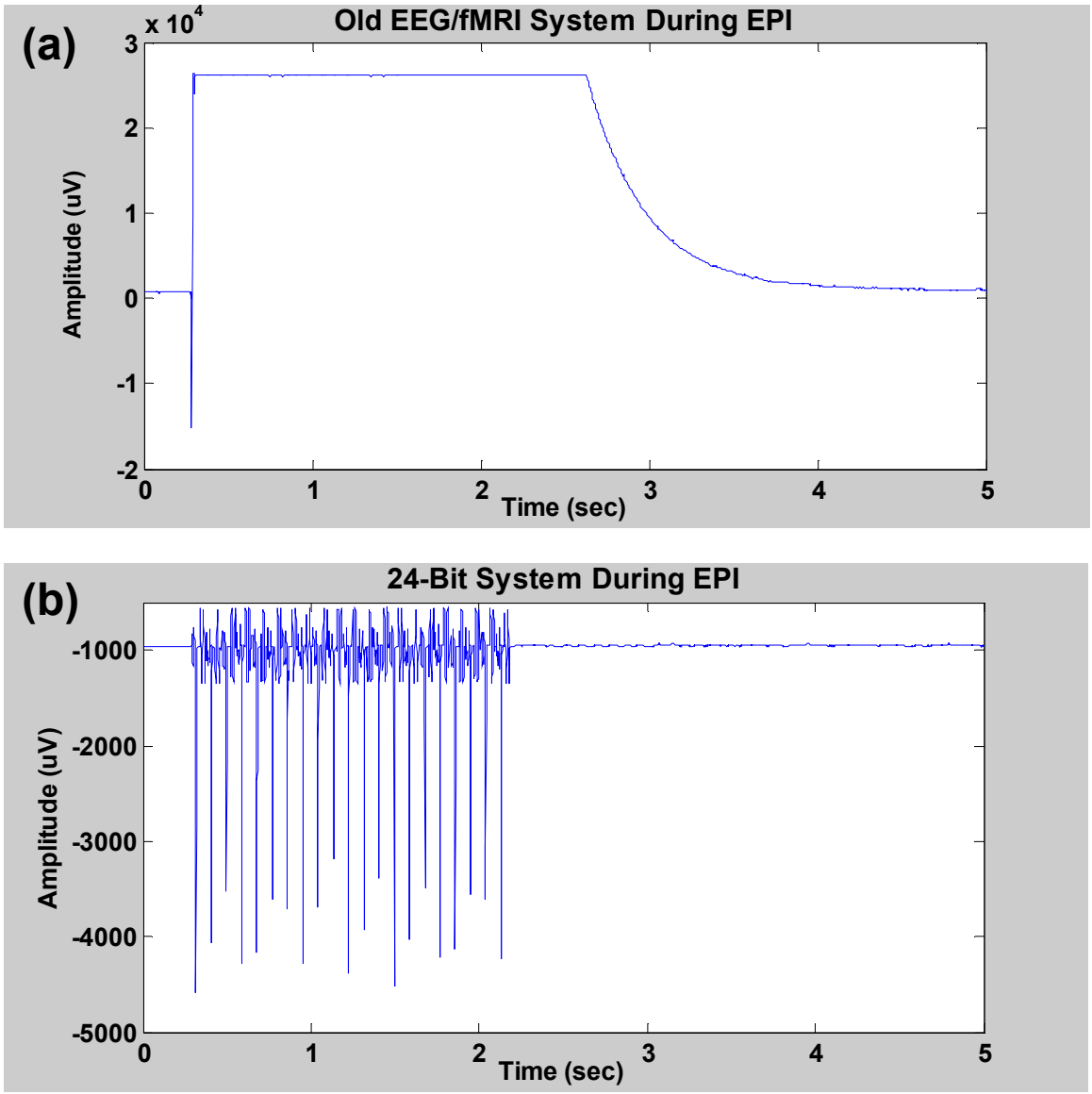

Figure 3.7. Amplifer recovery: (a) Traditional high-gain amplification system with AC-coupled input; (b) Low-gain DC amplifier.

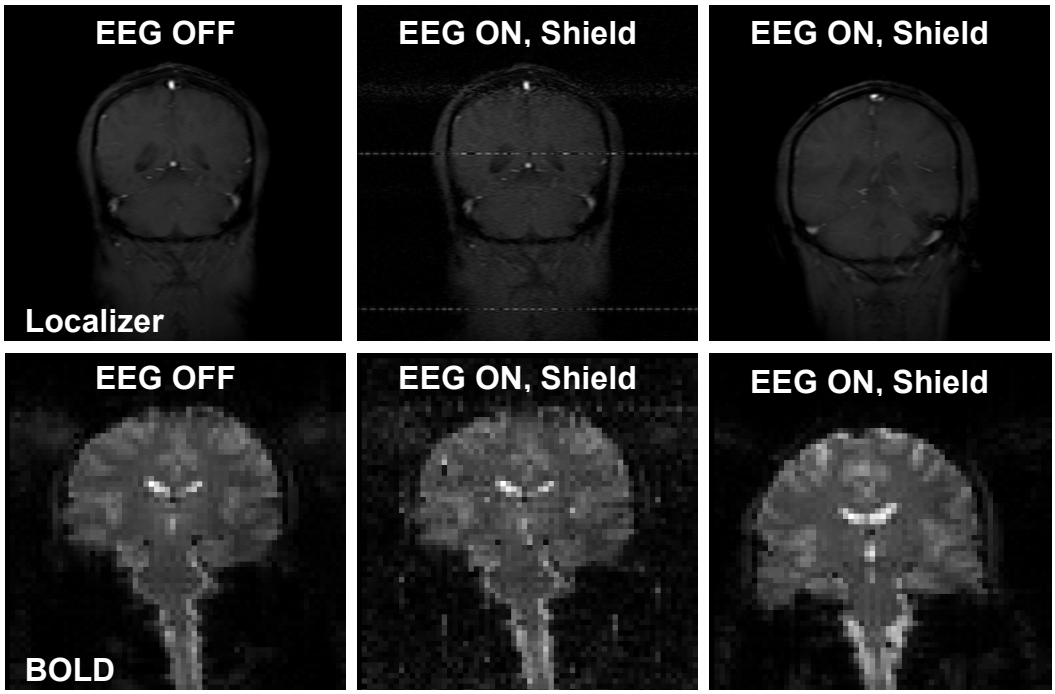

Figure 3.8. Image quality (a) without and (b) with RF shielding system.

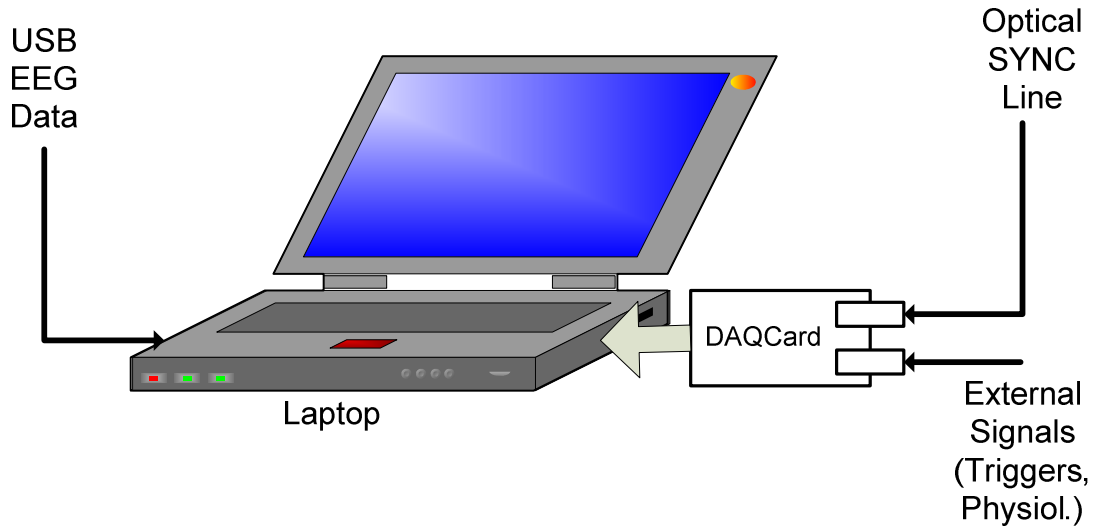

Figure 3.9. Block diagram of data acquisition and external signal integration architecture.

(a)

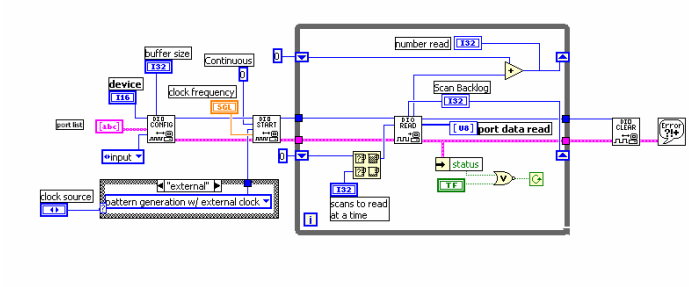

(b)

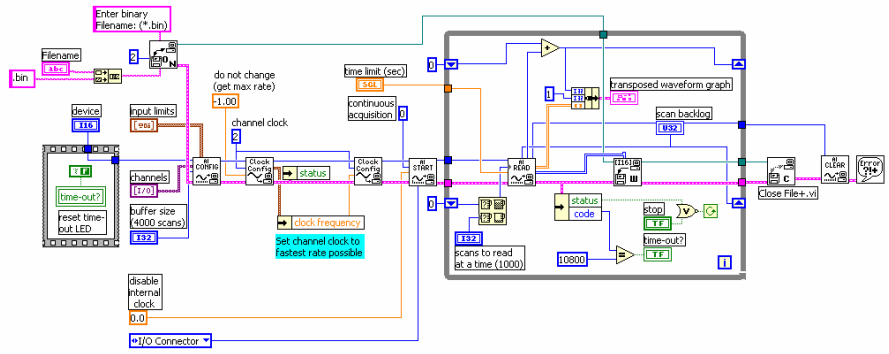

Figure 3.10. Block diagram for basic buffered acquisition LabView VI: (a) Digital buffered acquisition; (b) Analog buffered acquisition.

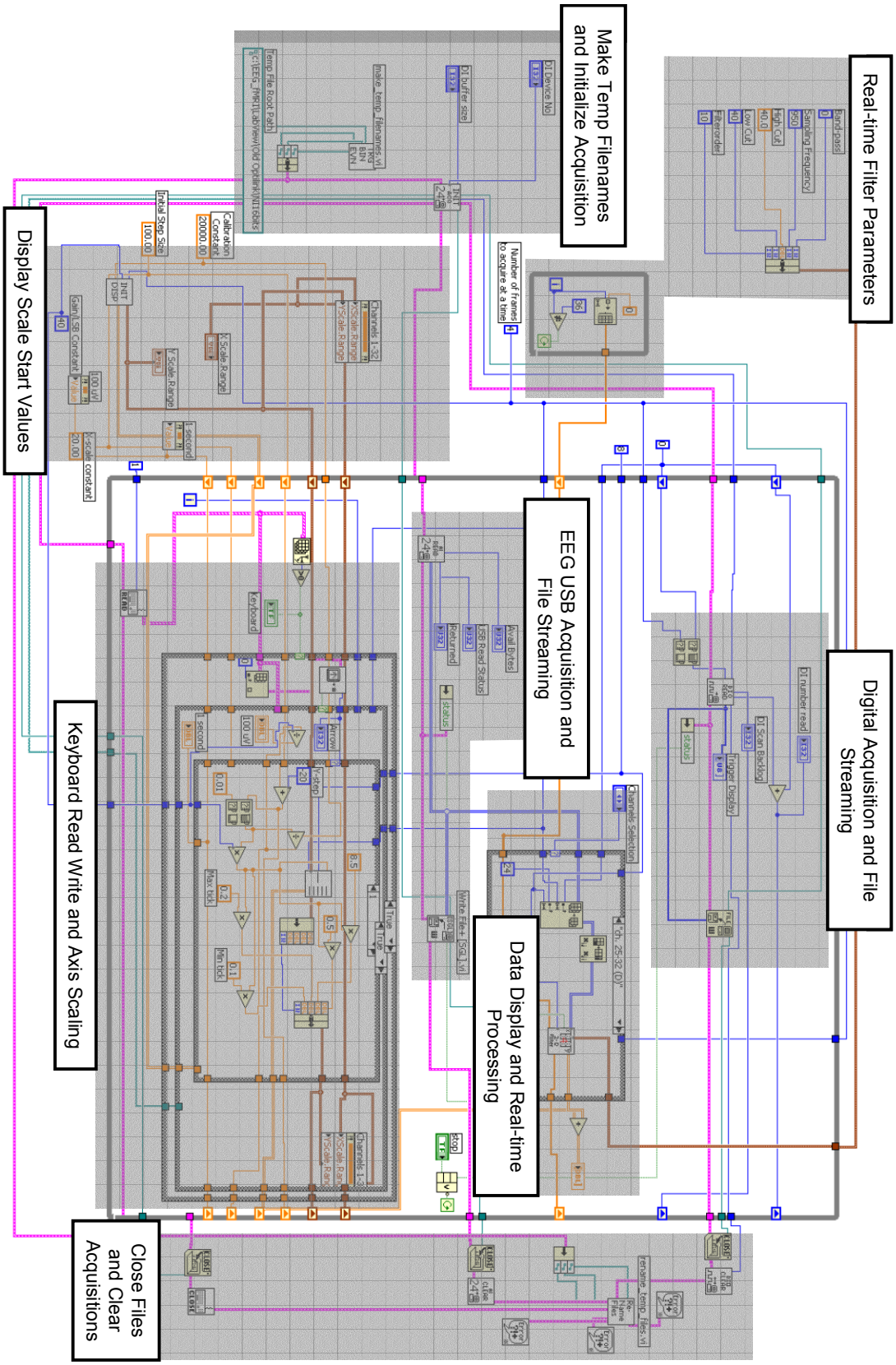

Figure 3.11. Top-level block diagram of EEG acquisition VI with functional annotations.

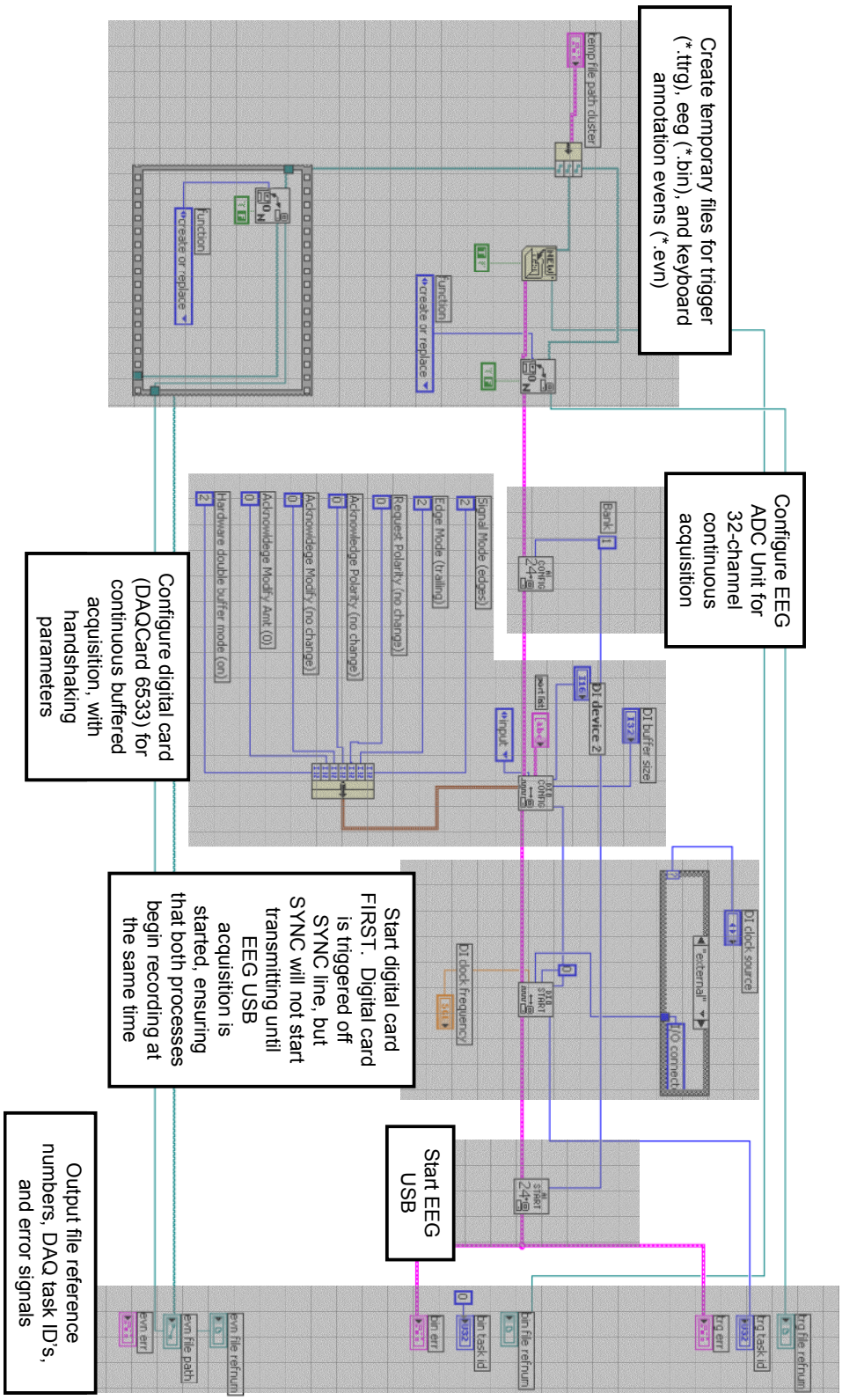

Figure 3.12. Annotated block diagram of "initialize_acquisition_24Bits.vi"

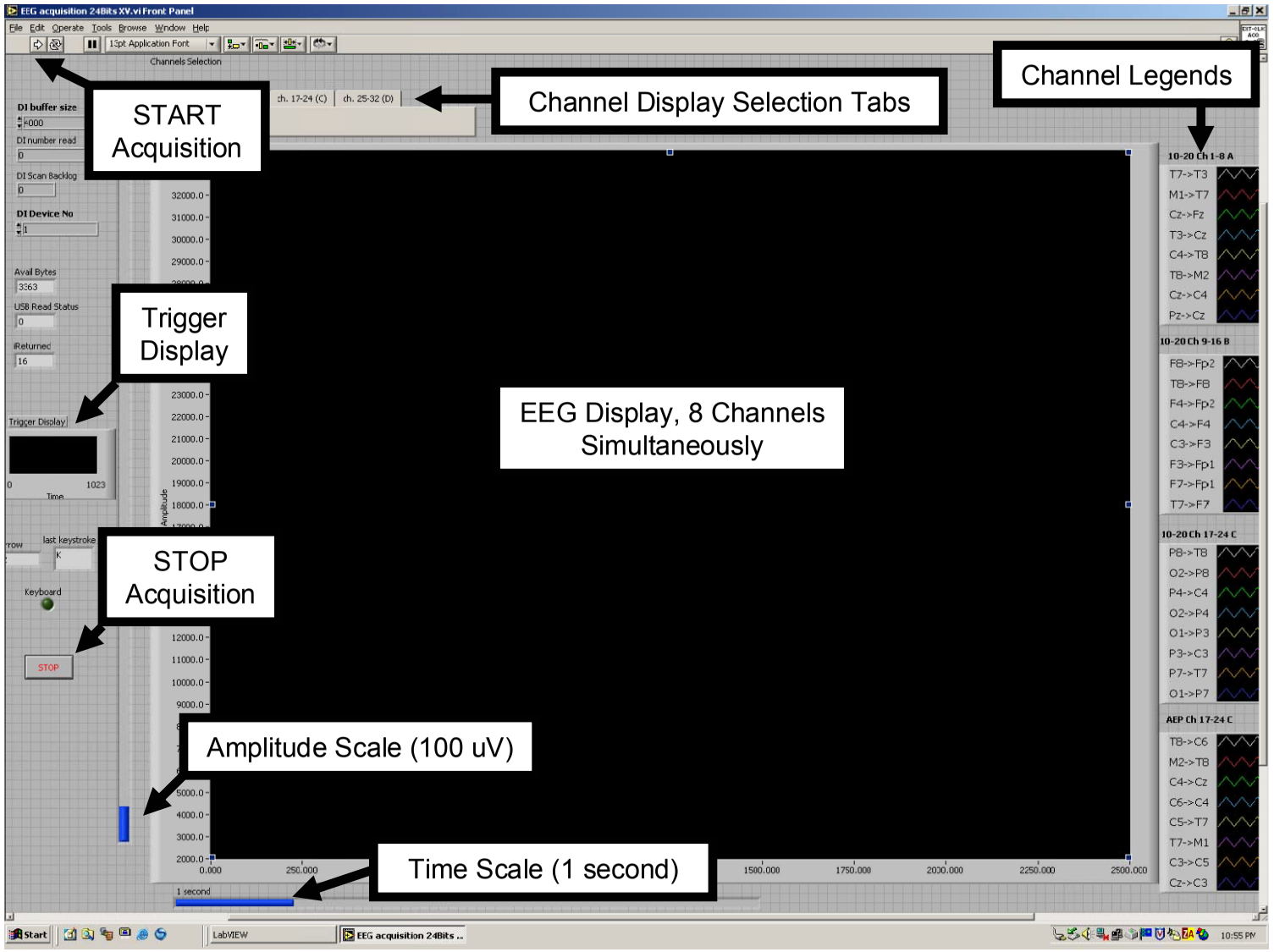

Figure 3.13. Front panel of EEG acquisition VI.

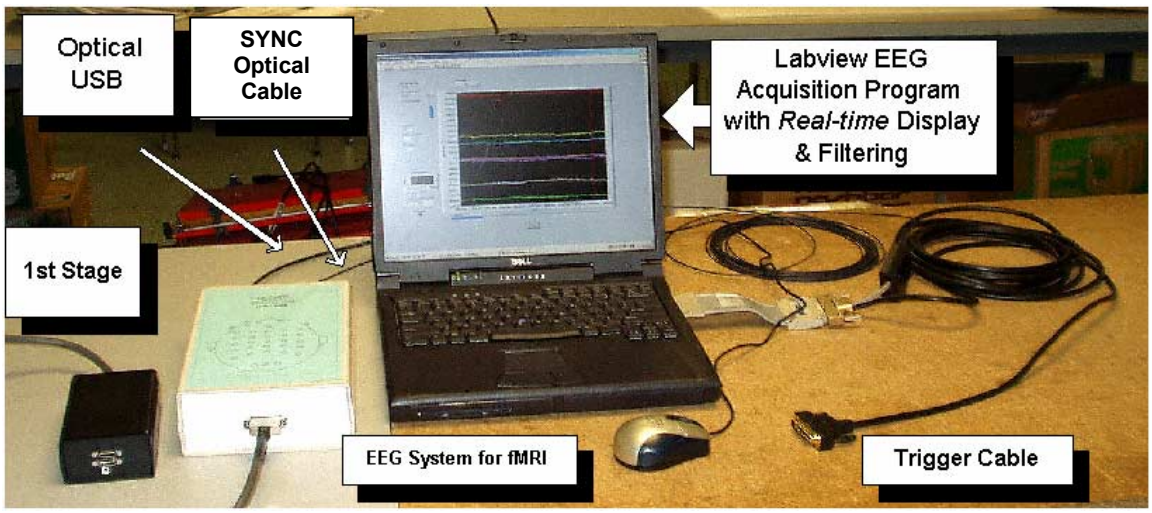

Figure 3.14 Complete system setup with amplifiers, EEG ADC acquisition unit, external signal card and cable assembly, and acquisition computer.

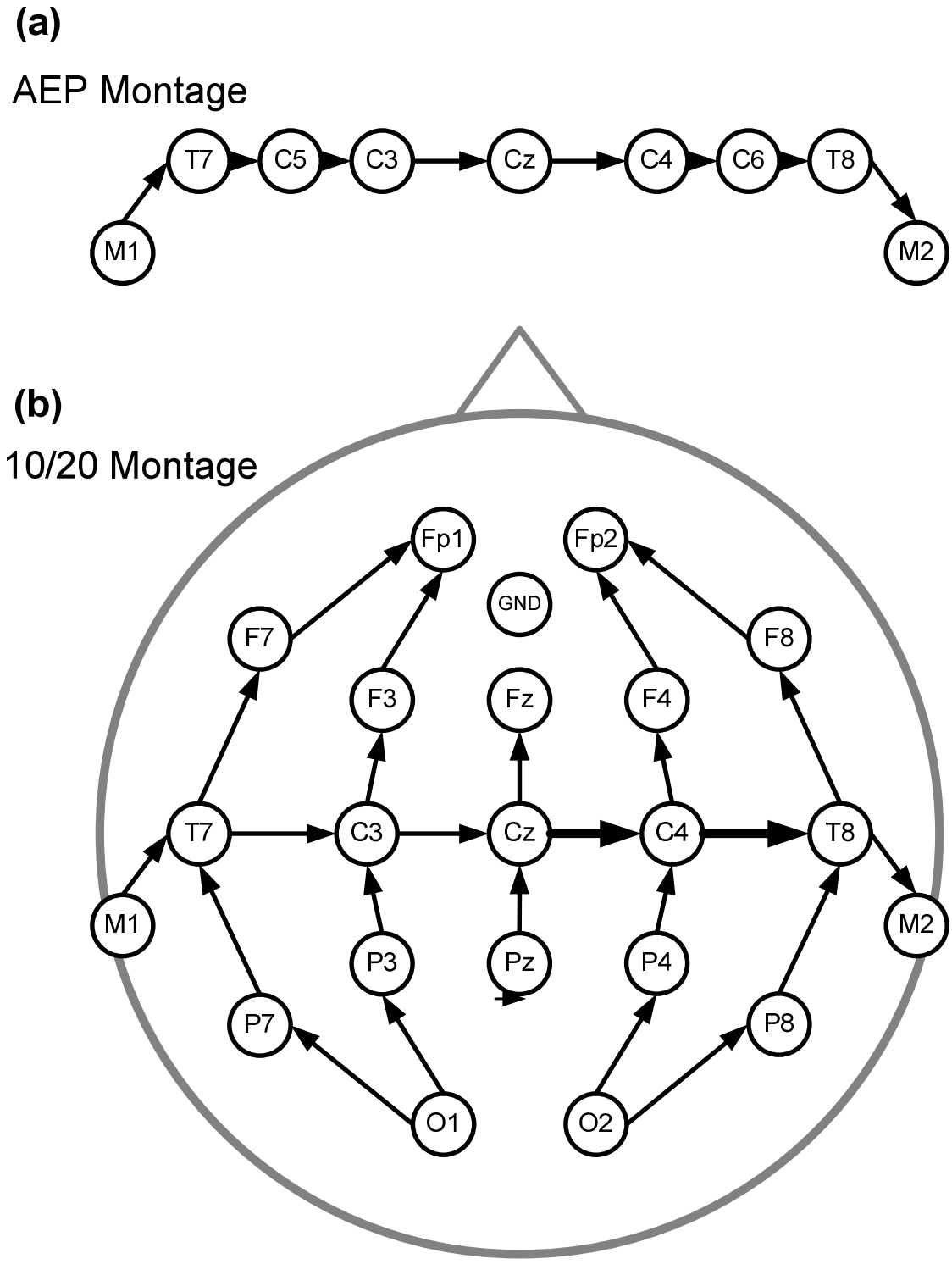

Figure 3.15. EEG-fMRI electrode montages: (a) Coronal AEP montage; (b) 10/20 montage.

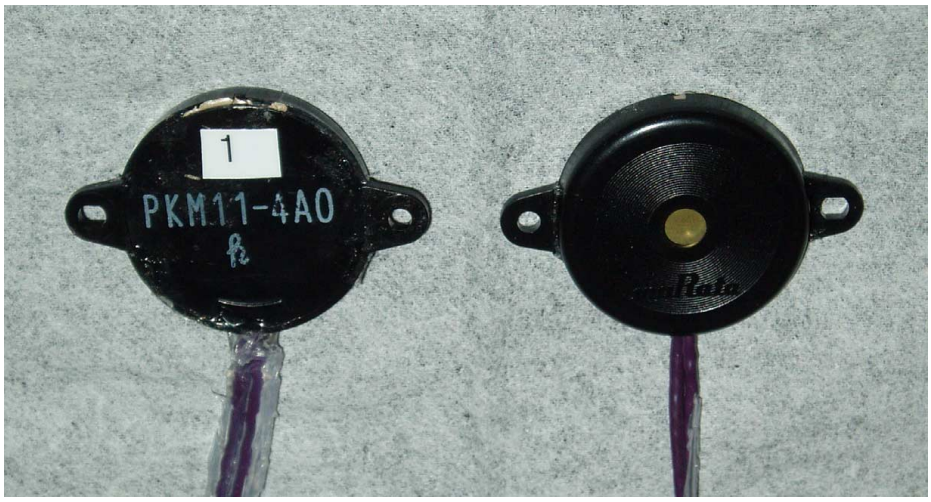

Figure 3.16. Motion sensors for EEG-fMRI.

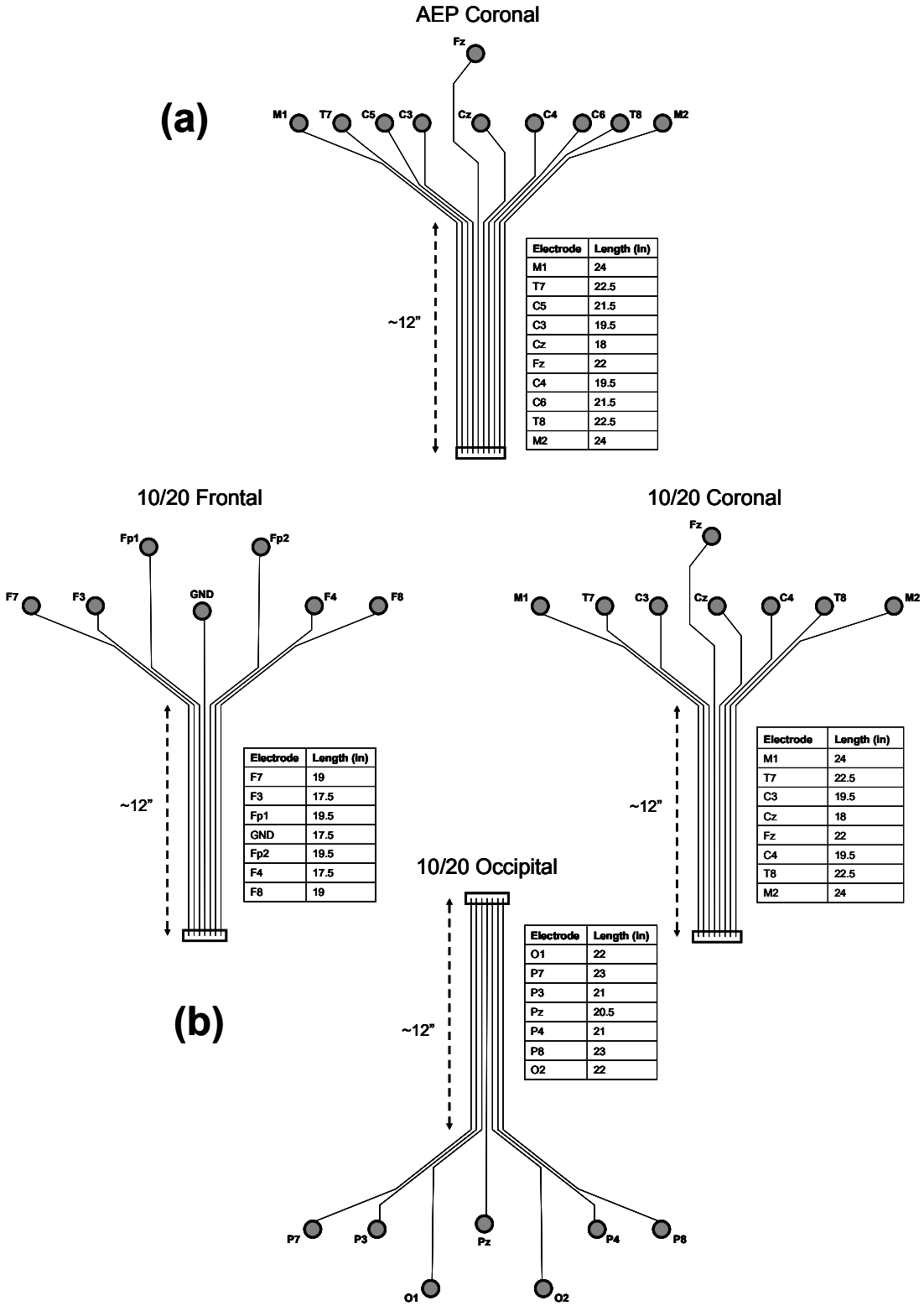

Figure 3.17. Ribbon cable EEG lead arrangements for (a) coronal montage and (b) 10/20 montage.

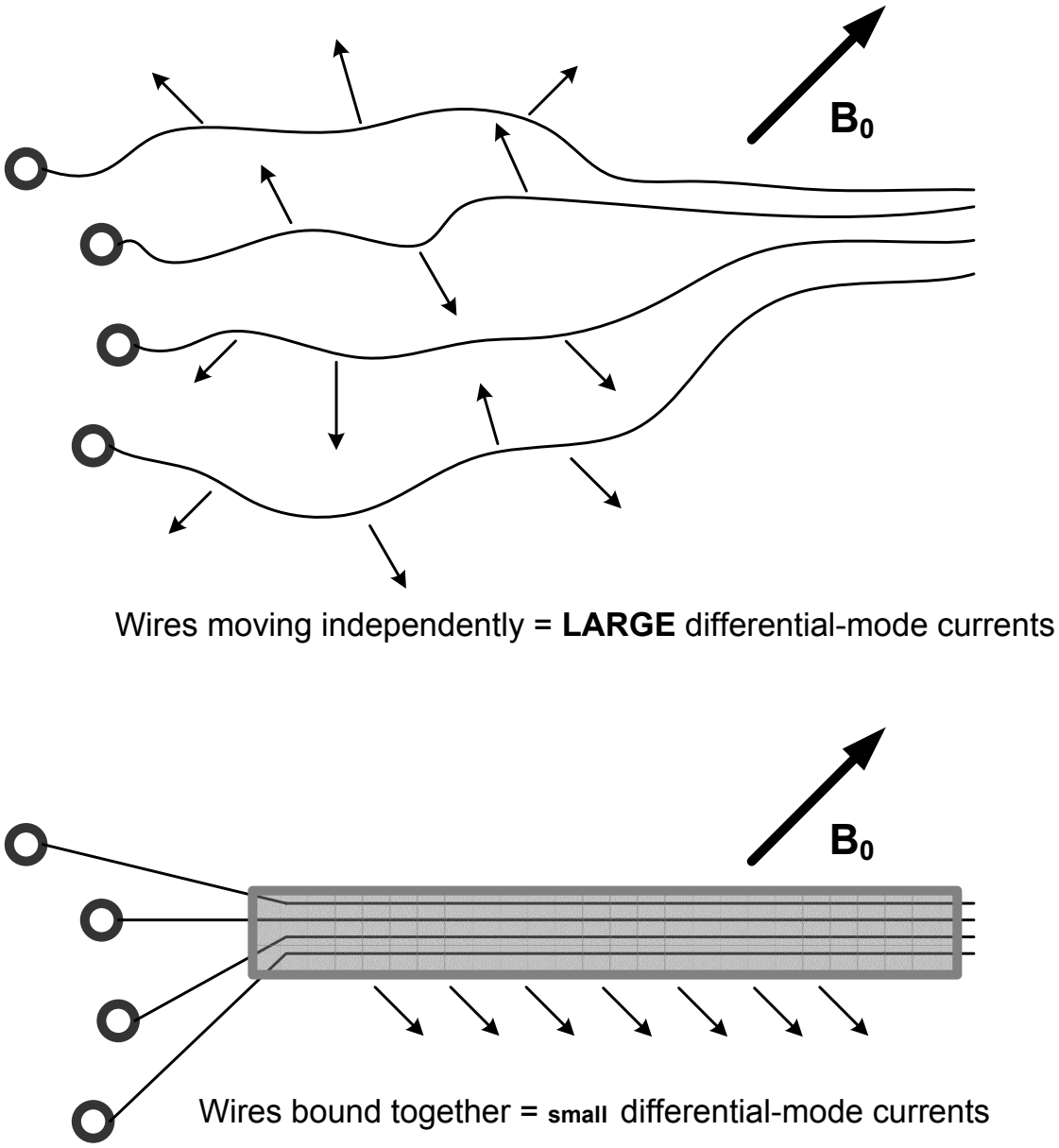

Figure 3.18. Ribbon cable EEG lead arrangement reduces electromechanical noise coupling.

Figure 3.19. EEG cap featuring conductive ink-based electrodes and integrated motion sensors.

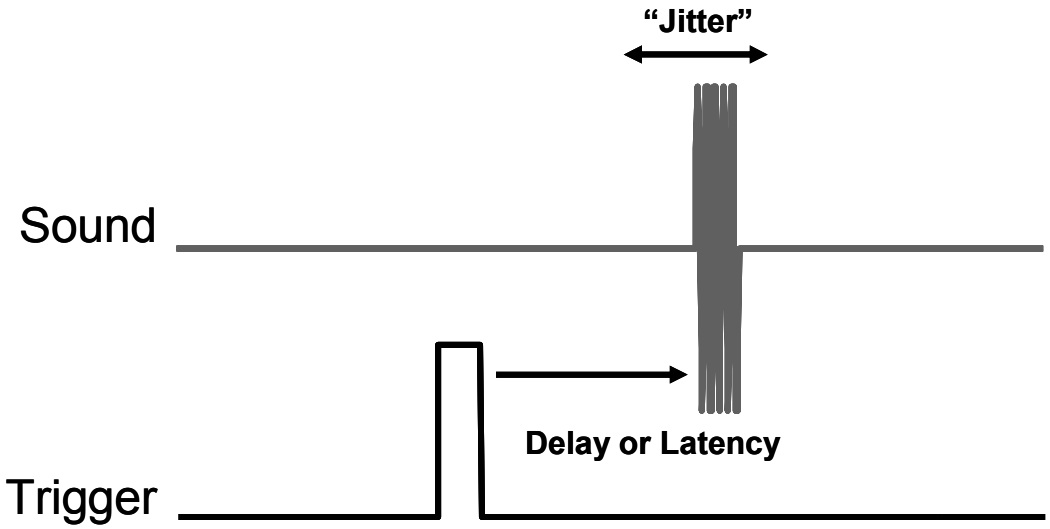

Figure 3.20. Stimulus presentation timing accuracy in terms of average delay (or latency) and jitter.

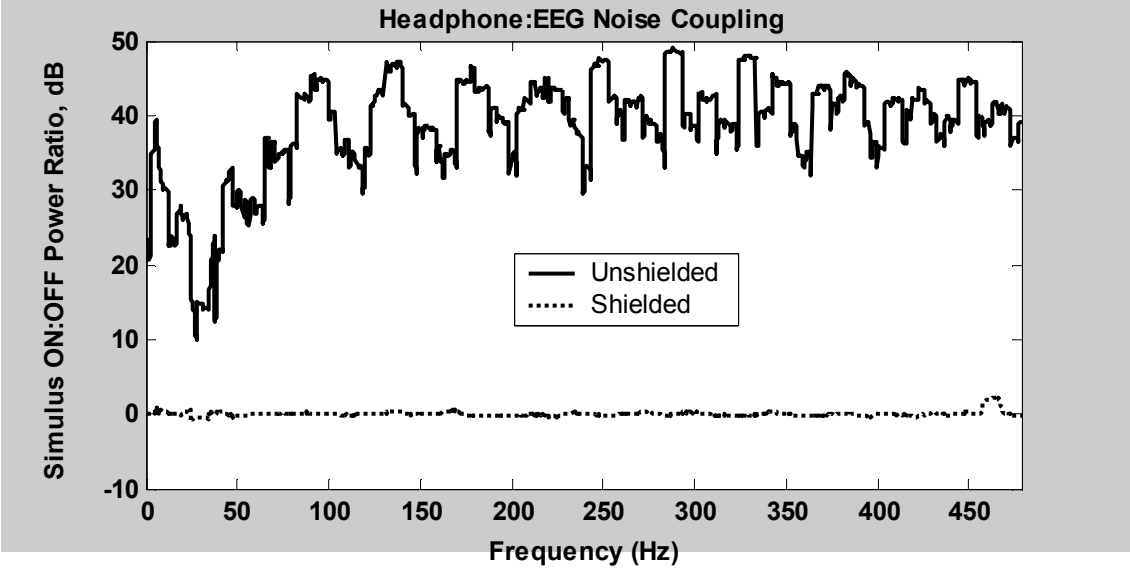

Figure 3.21. Headphone noise coupling, with and without shielding, across full EEG bandwidth

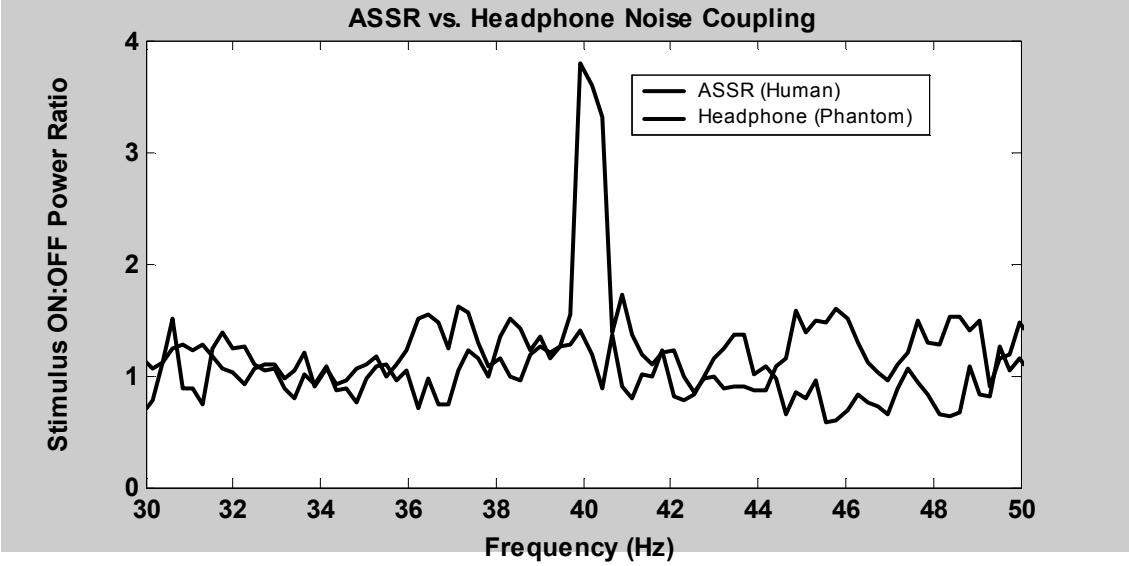

Figure 3.22. Comparison of auditory steady-state response (ASSR) to electrostatic headphone phantom recordings, illustrating that headphone shielding is effective.

Appendix 3A.1

Construction details for shielded chassis endplates and 21-pin micro-D filtered connectors

Shielded chassis endplates were precision cut using a T-Tech CircuitWorks 7000 PCB milling machine (T-Tech, Norcross, GA), using FR4 PCB material featuring double-sided 0.5-ounce copper (T-Tech BM-FR4-1DS, T-Tech, Norcross, GA; Figure 3A.1.a). Endplate shielding was enhanced by using copper tape (3M 3324-1, 3M, St. Paul, MN) to connect the two copper faces, and by soldering a row of copper mesh "teeth" (50007G; Amaco, Inc., Indianapolis, IN) to each edge of the endplates, which provide a light abrasion to the oxidation layer of the aluminum coating to ensure good contact (Figure 3A.1.b). A series of internal bulkheads were constructed, in a fashion similar to the endplates, in order to provide additional RF isolation for the ADC unit via filtered interconnects. Arrays of 70 nF feed-through filter capacitors (Tusonix 4404-002, Tusonix, Tuscon, AZ) were placed in each bulkhead to route critical input-output signal lines such as +/-12V power, amplified EEG signal lines, and +/-10V power, similar to those shown in Figure 3A.1.b. The Tusonix 4404-002 feed-through capacitor is rated with a capacitance of 50nF guaranteed minimum value (GMV), but in practice the parts supplied had a capacitance of 70.6 +/- 3.4 nF (from random sample of N=20).

Non-ferromagnetic 21-pin MIL-SPEC-83513 micro-D connectors (Microdot 624-0021-0001, Tyco Electronics, Harrisburg, PA) were modified by installing custom-made

1nF micro-D planar capacitor arrays (Syfer A055101X, 1 nF +/-20%, X7R ceramic, 5GOhm at 40 VDC, Syfer Technology Limited, Norwich, UK; Figure 3A.2.a). These capacitor arrays provide uniform pin-to-pin and pin-to-ground capacitance with low effective series resistance (ESR), and a geometry that provides input-output RF filtration as close to the chassis as possible, minimizing high-frequency RF susceptibility or radiation. The capacitor arrays were placed within approximately 2mm of the micro-D connector shell and soldered to each pin using indium solder (Indium Solder Research Kit, Alloy #4, Indium Corporation of America, Utica, NY) at approximately 185-degrees C to reduce the likelihood of temperature-related stress fractures in the capacitor arrays. The gap between the micro-D connector shell and the edge of the capacitor array was filled using a bare 14-gauge copper braid wire wrapped and soldered circumferentially to provide a 360-contact between the connector shell and capacitor array (Figure 3A.2.b). The amplifier analog ground was terminated to the amplifier chassis at pins 1, 10, 11, 12 and 21 of each micro-d input connector, with the corresponding pins on the capacitor arrays manufactured as ground pins (Figure 3A.2.c).

(a)

(b)

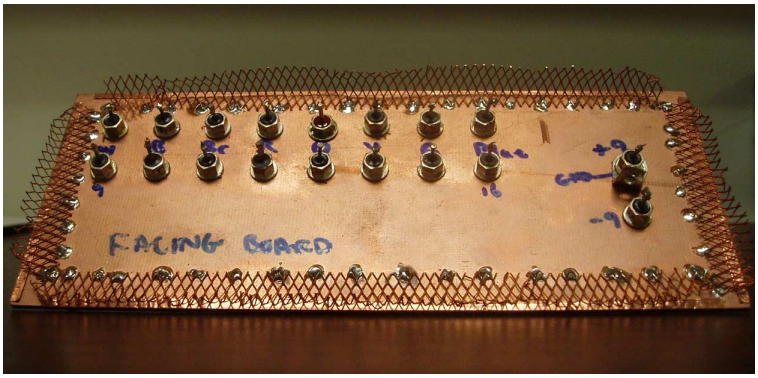

Figure 3A.1. Shielded Chassis Construction Details: (a) Double-sided copper endplates with precision-milled input-output connector ports; (b) RF bulkhead with feed-through capacitors and copper-mesh "teeth" to improve endplate-chassis connection.

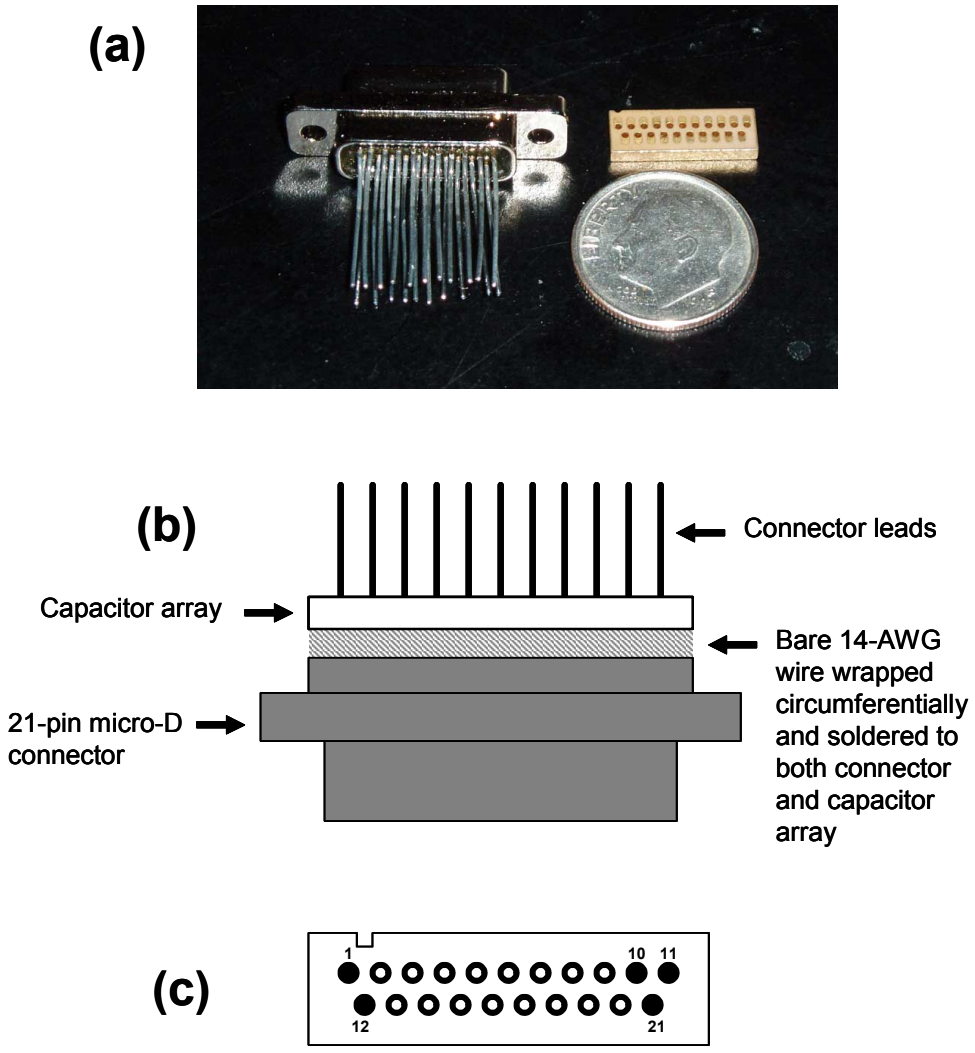

Figure 3A.2. 21-pin Micro-D Filtered Connector: (a) Photo of connector and capacitor array; (b) Schematic of capacitor array construction; (c) Location of ground-chassis connection at connector. Prior to order and delivery of capacitor arrays, the author constructed two prototype filtered connectors by individually soldering 1 nF 0405 surface mount ceramic capacitors between each of the 21 connector leads shown in (a) and the connector shell (not shown).

Appendix 3A.2.

Interconnects for integration of external digital or analog signals.

Adapter cable assemblies were constructed to provide interconnects for each external signal setup. Event triggers were recorded from the DB-25 parallel port of the stimulus presentation computer (described in Section 3.3). For the digital setup, the 8 parallel port data lines (D0-D7) were tied to the first 8 data lines of the 6533 (DIOA0-DIOA7). The optical SYNC signal from the ADC unit was received by an Agilent HFBR-2521 optical receiver (Agilent, Palo Alto, CA). The SYNC signal was connected to the REQ1 pin of the 6533 to drive externally-triggered acquisition. These connections were made using a National Instruments 68-pin backshell assembly (National Instruments 776832-01, National Instruments, Austin, TX). For the analog setup, the first four parallel port data lines (D0-D3) were connected to analog channels AI4-AI7, and the SYNC signal from the Agilent HFBR-2521 was tied to both PFI0 (TRIG1) and PFI7 (STARTSCAN) of the 6024E. Analog input channels AI0-AI3 were connected to pins 1 through 4 of a female DB-9 connector, to interface with the analog output lines from an Invivo Magnitude MRI-Compatible Patient Monitor (Invivo Research, Orlando, FL) corresponding to electrocardiogram (ECG), invasive pressure (P1), end-tidal CO2 (EtCO2), and pulse oximetry (SpO2) signals. A two-layer PCB board was constructed to integrate the optical receiver and input signals with a 68-pin connector to interface with the 6024E (National Instruments 777600-01, National Instruments, Austin, TX).

Appendix 3A.3

USB EEG interface functions.

3A.3.1. Overview of software drivers.

The software drivers for the USB EEG acquisition device consist of two pieces: A dynamic linked-library (DLL) for the FTDI FT245BM chipset used in the DLP USB interface ("FTD2XX.DLL"; Future Technology Devices International, Ltd., Glasgow, Scotland, UK; DLP Design, Inc., Allen, TX), and a second DLL written by Techen, Inc. ("TNusb.DLL" revision 110702; Milton, MA) to interface with the Ubicom SX48 (Ubicom, Inc., Mountain View, CA). Both files must be installed in the %SystemRoot%/System32 directory.

3A.3.2. Integration of USB DAQ functions from TNusb.DLL into LabView intermediate-level DAQ VI structure.

In Table 3A.3.1 below we describe four LabView intermediate-level DAQ VIs and their construction based on USB DAQ functions from TNusb.DLL. Most of these USB EEG VI's are constructed from simple LabView library function call, except for "AI Read 24-Bits.vi," which requires additional control structures to check the device status before reading data. A block diagram and description for "AI Read 24Bits.vi" is illustrated in Figure 3A.3.1.

Table 3A.3.1. LabView intermediate-level DAQ VIs and USB DAQ functions from TNusb.DLL

VI Name	AI Config 24Bits
Purpose	Configure EEG acquisition

USB Commands Used	unsigned long_UsbConfig@16(unsigned long iBank, unsigned long iCount, unsigned long iadcCH, unsigned long iFilter);
Description	iBank (1-8): Specifies SX48 memory location where configuration setting will be stored. Operates much like the "process ID" used in NI DAQ VIs. iCount (0-65535): Number of samples to acquire. "0" corresponds to continuous recording. Set to "0" in AI Config 24Bits. iadcCH (1-5): ADC channel to take data from. "5" corresponds to multiplexing through all four channels on each chip, resulting in 32 channels total.
VI Name	**AI Start 24Bits**
Purpose	Start EEG acquisition
USB Commands Used	unsigned long_UsbStart@8(unsigned long iBank, unsigned long iCount);
Description	iBank (1-8): Specifies SX48 memory location where configuration setting have been stored during "AI Config 24-Bits" process. Operates much like the "process ID" used in NI DAQ VIs. iCount (0-65535): Number of samples to acquire. "0" corresponds to continuous recording. Set to "0" in AI Config 24Bits.
VI Name	**AI Read 24Bits**
Purpose	Read EEG data in buffered acquisition
USB Commands Used	unsigned long UsbStatus(unsigned long *AvailableBytes); unsigned long_UsbRead@12(long_*Data, unsigned long *iReturned, unsigned long *AvailableBytes);
Description	AvailableBytes: Available bytes in buffer. Data: Data packet consisting of a 16x10 array of 32-bit

	signed integers. Only first 8 columns of array contain EEG data. In full multiplexing mode (iadcCH=5), each packet corresponds to 4 time points of 32 channels. AI Read 24Bits.vi re-packages each packet into a 4 (time) x 32 (channel) array.
VI Name	**AI Clear 24Bits**
Purpose	Stop EEG acquisition
USB Commands Used	Unsigned long_UsbStop@0(void);
Description	Required for proper acquisition termination. If VI is terminated without using this function, EEG ADC unit may have to be re-booted to resume normal operation.

3A.3.3. Status Messages

The FTD2XX.DLL driver has a series of status messages ranging from 0 to 17. The TNusb.DLL driver wrapper has an additional series of status messages ranging from 256 to 263 and 999. All the status message definitions are listed below.

Table 3A.3.1. Status Messages.

Message	Code
FTD2XX.DLL Status Messages:	
FT_OK	0
FT_INVALID_HANDLE	1
FT_DEVICE_NOT_FOUND	2
FT_DEVICE_NOT_OPENED	3
FT_IO_ERROR	4
FT_INSUFFICIENT_RESOURCES	5
FT_INVALID_PARAMETER	6
FT_INVALID_BAUD_RATE	7
FT_DEVICE_NOT_OPENED_FOR_ERASE	8
FT_DEVICE_NOT_OPENED_FOR_WRITE	9

FT_FAILED_TO_WRITE_DEVICE	10
FT_EEPROM_READ_FAILED	11
FT_EEPROM_WRITE_FAILED	12
FT_EEPROM_ERASE_FAILED	13
FT_EEPROM_NOT_PRESENT	14
FT_EEPROM_NOT_PROGRAMMED	15
FT_INVALID_ARGS	16
FT_OTHER_ERROR	17
TNusb.DLL Status Messages:	
TN_DeviceNotOpen	256
TN_ParameterLimit	257
TN_BytesWrittenError	258
TN_DeviceAlreadyOpened	259
TN_NoDataAvailable	260
TN_NumAvailableBusy	261
TN_SYNCBytesNotFound	262
TN_AlreadyProcessing	263
TN_BufferOverRun	999

Message 999 indicates that the TNusb.DLL internal 2 million byte buffer has over flown. If this status message is received, no additional data can be read from the buffer before a new “start” command has been issued.

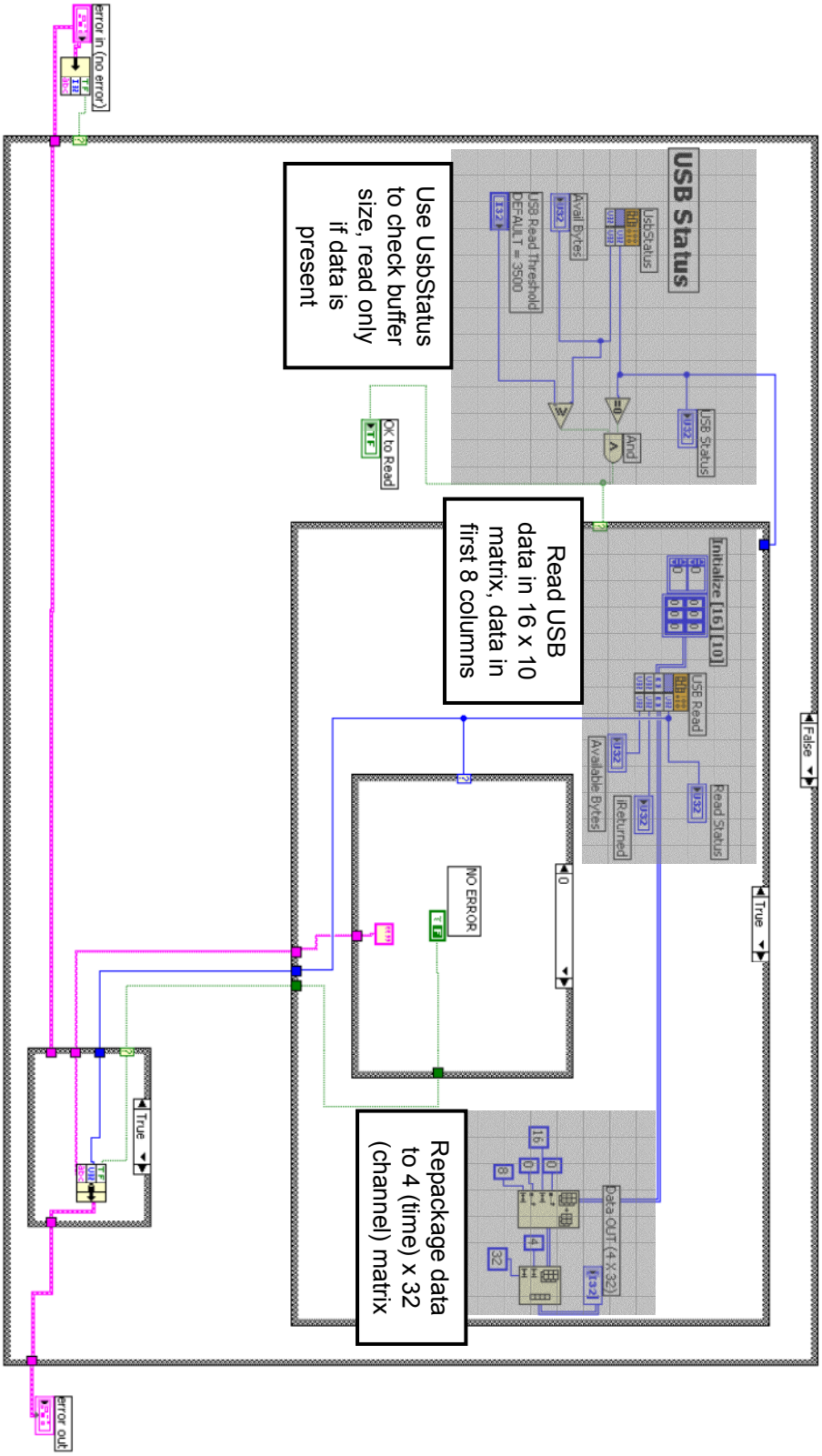

Figure 3A.3.1. Block diagram of for “AI Read 24Bits.vi”

Appendix 3A.4

Electrode construction details.

Carbon fiber wires ("Fiber-Ohm;" Marktek, Inc., Chesterfield, MO), with 7 Ohms/inch resistance (276 Ohms/meter), were bonded to Gereonics Ag/Ag-Cl electrode bodies (Gereonics, Inc., Solana Beach, CA) using conductive epoxy (Circuit Works CW2400; Chemtronics, Kennesaw, GA). These electrode-to-wire connections were mechanically reinforced by using an adhesive sealant (Shoe Goo, Eclectic Products, Inc., Pineville, LA) to form a protective sheath around the conductive epoxy joint (Figure 3A.4.a). Electrode wires were arranged into a ribbon and then bonded together with a double-sided coating of RTV silicone (MG Chemicals 1015-85, MG Chemicals, Surrey, British Columbia, Canada), as shown in Figure 3A.4.b. A PCB adapter was constructed to provide connections between the 21-pin MIL-SPEC-83513 micro-D connectors (Figure 3A.4.d; Microdot 8-1532027-4, Tyco Electronics, Harrisburg, PA) and short segments of ribbon cable, which were then bonded to the carbon fiber wires using standard cable crimp connectors (Figure 3A.4.c; Gardner Bender 10-123, Gardner Bender, Milwaukee, WI).

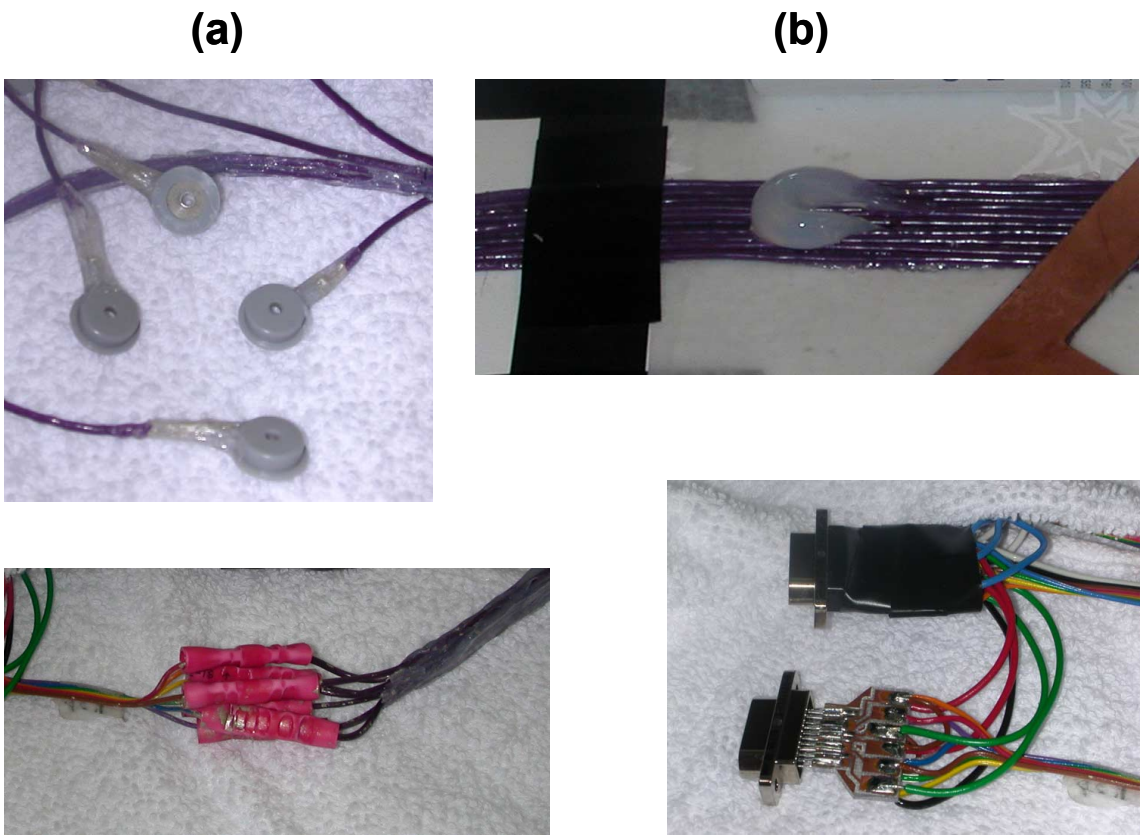

Figure 3A.4. Electrode construction details: (a) Electrode-to-wire connections made with conductive epoxy and mechanically reinforced with adhesive sealant; (b) Bonding of ribbon cable using RTV silicone; (c) Butt-splice connectors bonded with conductive epoxy to join carbon fiber wires with copper braid ribbon cable from 21-pin micro-D connector (d) PCB adapter to interface with 21-pin micro-D connector.

Appendix 3A.5

Stimulus Timing Accuracy

Stimulus timing accuracy for a variety of hardware and software configurations were tested using a modified version of the NeuroBehavioral Systems Sound Card Latency Analyzer (SCLA) software distribution (release date ca. January 2004, NeuroBehavioral Systems, Carpinteria, CA). For many of the experimental protocols

used in our laboratory, precise timing between fMRI acquisitions and stimulus delivery were desired. If the MRI system and Presentation system operate independently during a scan, small systematic differences between the MRI system timing and Presentation timing could produce large accumulated timing errors during longer fMRI scans. To enforce precise timing between fMRI acquisitions and stimulus delivery, presentation scripts were developed to provide an external trigger to the MRI system via the parallel port. Since Presentation handles port output (i.e., triggers) with interrupts, there was concern that use of multiple trigger types (e.g., stimulus triggers vs. scan triggers) might influence stimulus timing. For this reason the SCLA testing protocol was modified to give insight into how different configurations of stimulus and scan triggers might influence timing accuracy. Three trigger configurations were tested, as illustrated in Figure 3A.5.1: (1) Sending only stimulus triggers and no scan triggers (NO_SCAN); (2) Sending stimulus and scan triggers simultaneously (SIMULTANEOUS); (3) Delaying stimulus triggers by 200 msec after scan triggers (STIM_DELAY). In addition, since specific computer configurations can influence timing, several hardware and software configurations were tested: (1) Different laptops (an IBM Thinkpad T40 running Windows XP vs. a Dell Latitude C610 running Windows 2000), (2) Different versions of Presentation (0.47 vs. 0.76), and (3) Different sound cards (laptop built-in sound or external Echo Indigo PCMCIA card).

Recording hardware were set up according to the suggested SCLA protocol, with one computer used to provide the stimuli, and another to record the stimuli and triggers using its audio input jack: a 1/8" stereo audio jack was connected to the line-in input of recording computer, with one channel set to the audio channel and the other tied to the

Data0 pin of the presentation computer (Figure 3A.5.2). A 10 msec 2 KHz sine wave was used as the stimulus, with a stimulus trigger duration of 5 msec. Each stimulus/stimulus-trigger/scan-trigger packet was presented at an interval of 500 msec, with 100 trials per experimental condition. The stimulus and trigger outputs were recorded as WAV files from the sound input port using the Windows sound recorder utility. The data were analyzed using Matlab (Mathworks, Natick, MA). Onset timing for stimuli and stimulus triggers were detected by thresholding (threshold value of 0.2 for data values ranging from -1 to +1), and the mean (delay) and standard deviation (jitter) were computed for the difference between stimulus time and stimulus trigger time for each experimental condition. These results are summarized in Table 3A.1. A number of important inferences can be made from these data:

1. Stimuli should be delayed relative to scan triggers if possible. Across all conditions, both average delay and jitter were orders of magnitude larger when scan and stimulus triggers were delivered simultaneously. When stimuli were delayed relative to scan triggers, delay and jitter values were similar to those without scan triggers.
2. Use of the Echo Indigo PCMCIA sound device added approximately 1 msec to the average delay compared with onboard sound devices, but jitter values remained similar when averaged across laptops and remained below 1 msec. Occasional sound stimulus events were omitted when using this card with Presentation 0.76, but this occurred only for ~1% of trials presented with this card and software version.

Table 3A.1. Average delay and jitter (std. dev.) values for different presentation hardware and software configurations. "CrystalWDM" and "SoundMAX" refer to chipsets for built-in laptop sound.

Computer	Sound Device	Pres. Ver.	Stimulus Condition	Avg. Delay	Jitter
LatitudeC610	CrystalWDM	0.76	NO_SCAN	-0.485	0.057
LatitudeC610	CrystalWDM	0.76	SIMULTANEOUS	-26.245	2.826
LatitudeC610	CrystalWDM	0.76	STIM_DELAY	-0.588	0.412
LatitudeC610	Echo Indigo	0.47	NO_SCAN	-23.722	0.831
LatitudeC610	Echo Indigo	0.47	SIMULTANEOUS	-25.845	0.849
LatitudeC610	Echo Indigo	0.47	STIM_DELAY	-25.461	0.848
LatitudeC610	Echo Indigo*[2]	0.76	NO_SCAN	-1.566	0.223
LatitudeC610	Echo Indigo*[4]	0.76	SIMULTANEOUS	-30.181	2.655
LatitudeC610	Echo Indigo	0.76	STIM_DELAY	-1.789	0.09
ThinkpadT40	Echo Indigo*[1]	0.76	NO_SCAN	-1.869	0.256
ThinkpadT40	Echo Indigo	0.76	SIMULTANEOUS	-23.29	0.132
ThinkpadT40	Echo Indigo	0.76	STIM_DELAY	-1.914	0.495
ThinkpadT40	SoundMAX	0.76	NO_SCAN	-0.801	0.215
ThinkpadT40	SoundMAX	0.76	SIMULTANEOUS	-25.553	0.074
ThinkpadT40	SoundMAX	0.76	STIM_DELAY	-0.93	0.062

* = On these trials, sound stimuli were missing for 2, 4, or 1 out of 100 stimuli presented.

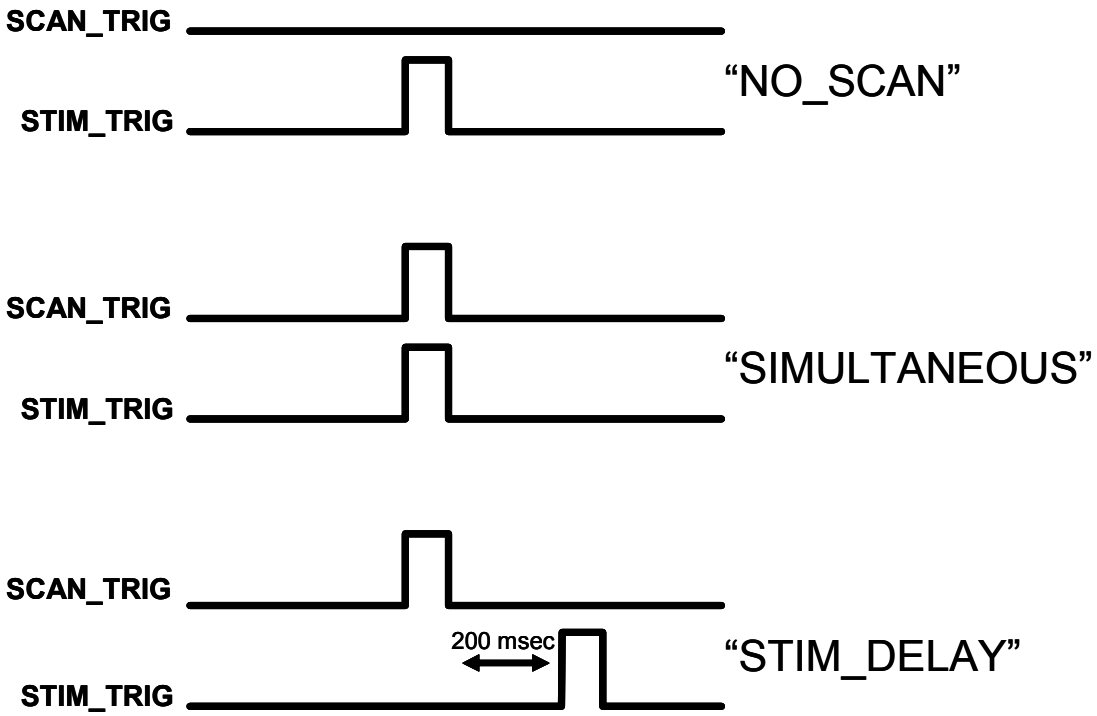

Figure 3A.5.1. Timing configurations for stimulus and scan triggers.

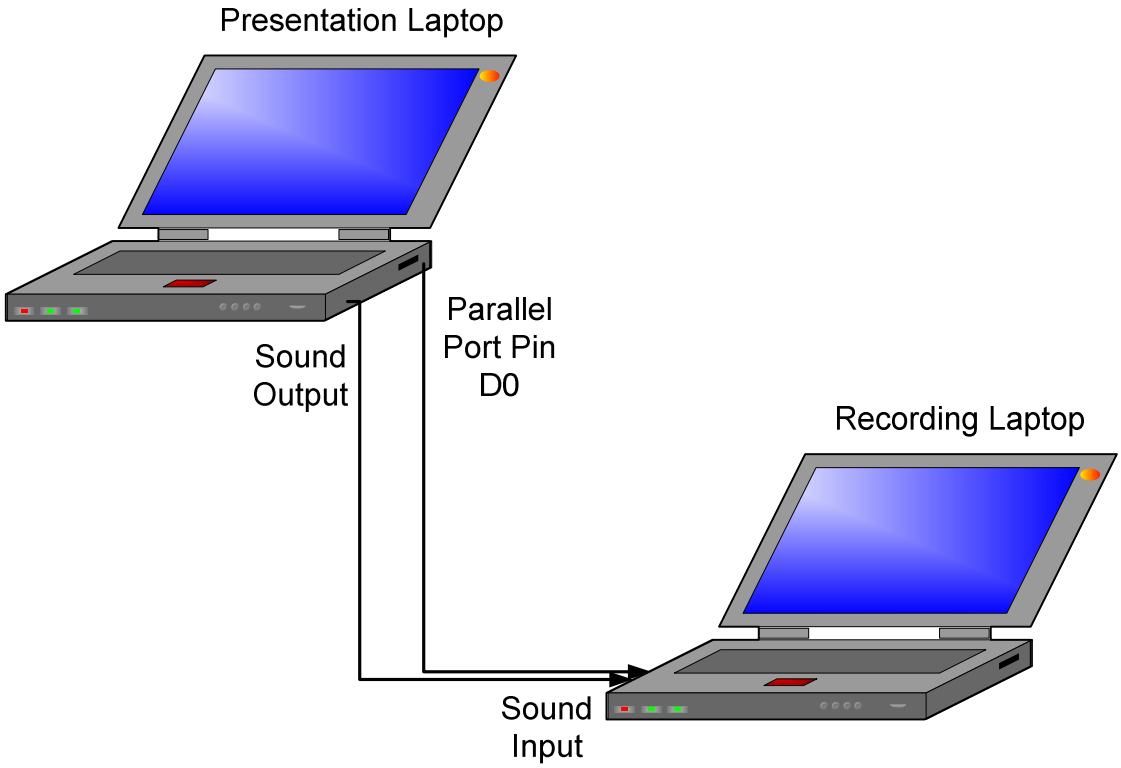

Figure 3A.5.2. Hardware connections for SCLA protocol.

Appendix 3A.6
Construction details for electrically-shielded acoustically-attenuating electrostatic headphones

3A.6.1. Modification of sound attenuating earmuffs

Sound-attenuating earmuffs (Silenta Ergomax, Oy Silenta Ltd., Finland) were modified to enclose the electrostatic headphone elements from a set of Koss ESP-950 headphones (Koss Corp., Milwaukee, WI). Internal molding posts and sharp edges were filed down to prevent abrasion or damage to the headphone elements. An aperture was cut at the bottom of each headphone enclosure, approximately 1.5 x 4.5 cm in dimensions, to allow the electrical contacts of the electrostatic headphone elements to fit inside the enclosure. A plastic box enclosure, approximately 2 x 5 x 5 cm in dimensions, was fused to the aperture using hot melt glue to protect the electrical contacts of the headphone elements. A ¼" hole was drilled in the outer aspect of each plastic box to allow cabling to pass through. The ear-cushion ring assembly was modified by placing a hard plastic mesh backing material (with ~1/8" holes) over the ear aperture, covering the external (ear side) of the hard plastic mesh with speaker cloth. This modification was

made to prevent direct contact between the study subject and headphone elements. The modified enclosure is shown in Figure 3A.6.1.

3A.6.2. Replacing stock cables with double-shielded cables

The electrostatic headphone elements were removed from a set of Koss ESP-950 headphones (Figure 3A.6.2). The first 6 feet of stock cable attached to the headphone elements were replaced with double-shielded (braid over foil) computer cabling, taking care to leave approximately 1 cm of both braid and foil shield exposed near the headphone elements. The double-shielded cables were threaded through the holes in the sound-attenuating enclosures, and then re-connected with headphone elements according to the wiring chart shown in Figure 3A.6.3. An additional 6 feet of stock headphone cable was spliced to the double-shielded cabling to provide connection with the amplifier unit, with a small plastic junction box to protect the cable splicing (Figure 3A.6.4). Heyco strain relief connectors (Bolt Products, Inc., City of Industry, CA) were also used to reinforce the cable connections. The computer cable shield was extended along the length of the stock headphone cable with a single 14-AWG wire, to allow for termination to the amplifier shield (described below). The stock headphone cable and ground cable were bound together and protected by a spiral cable wrap attached to the junction box with hot melt glue (Figure 3A.6.4).

3A.6.3. Electrical insulation for electrostatic headphone elements

Large diameter shrink-tubing was used to insulate the electrical connectors of the headphone elements. A single layered thin plastic membrane was wrapped around each

headphone element and sealed to the large diameter shrink tubing using double-sided tape. A small 1 x 1 cm piece of electrician's tape was used to reinforce the thin plastic over the upper portion of the headphone element's electrical connector that remained unprotected by the large diameter shrink tubing. These elements are illustrated in Figure 3A.6.5.

3A.6.3. Conductive mesh fabric shield for electrostatic headphone elements

The electrostatic headphone elements were shielded by placing a conductive fabric sock constructed from silver-coated sheer nylon (Less EMF Cat. #A209, Less EMF Inc., Albany, NY) over the headphone element. The conductive fabric was chosen for its low resistivity (<5 Ohms/square) and low acoustic absorption. The conductive mesh sock was sewn together circumferentially, except for a small hole where connector wires were allowed to pass. The fabric sock was carefully terminated to the double-shielded computer cable using copper tape applied in two stages. First, the open end of the fabric sock was wrapped circumferentially around the inner foil shield, which was secured with a wrapping of copper tape. Second, the braid shield was distributed circumferentially around that first layer of copper tape, and then secured in place with a second layer of copper tape. The shielded electrostatic elements were carefully inserted into the earmuff enclosure, a thin ring of plastic foam was placed around the outside edge of the electrostatic element to prevent abrasions from the ear cushion, and the ear cushion was snapped into place. Heyco strain relief connectors were used to secure the double-shielded computer cable to the earmuff enclosure.

3A.6.4. Power, grounding, sound input, and amplifier shield connections

Power was provided by a single 9.6V 1800 mA-hour Ni-Cd battery (Radio Shack Corp., Fort Worth, TX). Since the battery is ferromagnetic, it was kept outside the shielded room and brought in through the penetration panel through an unfiltered BNC port, connecting the positive terminal of the battery to the BNC signal conductor and the negative terminal of the battery to the BNC shield. In this way the power reference of the headphone amplifier was connected to the shielded room reference. A copper mesh shield was constructed for the Koss amplifier system with a interconnect system to connect the headphone shield cable to the amplifier shield, which was in turn connected to the battery/shielded-room reference. This arrangement is depicted in Figure 3A.6.6. Sound was delivered using the 1/8" stereo jack at the front of the Koss amplifier unit, brought into the shielded room through a filtered DB-9 in the penetration panel.

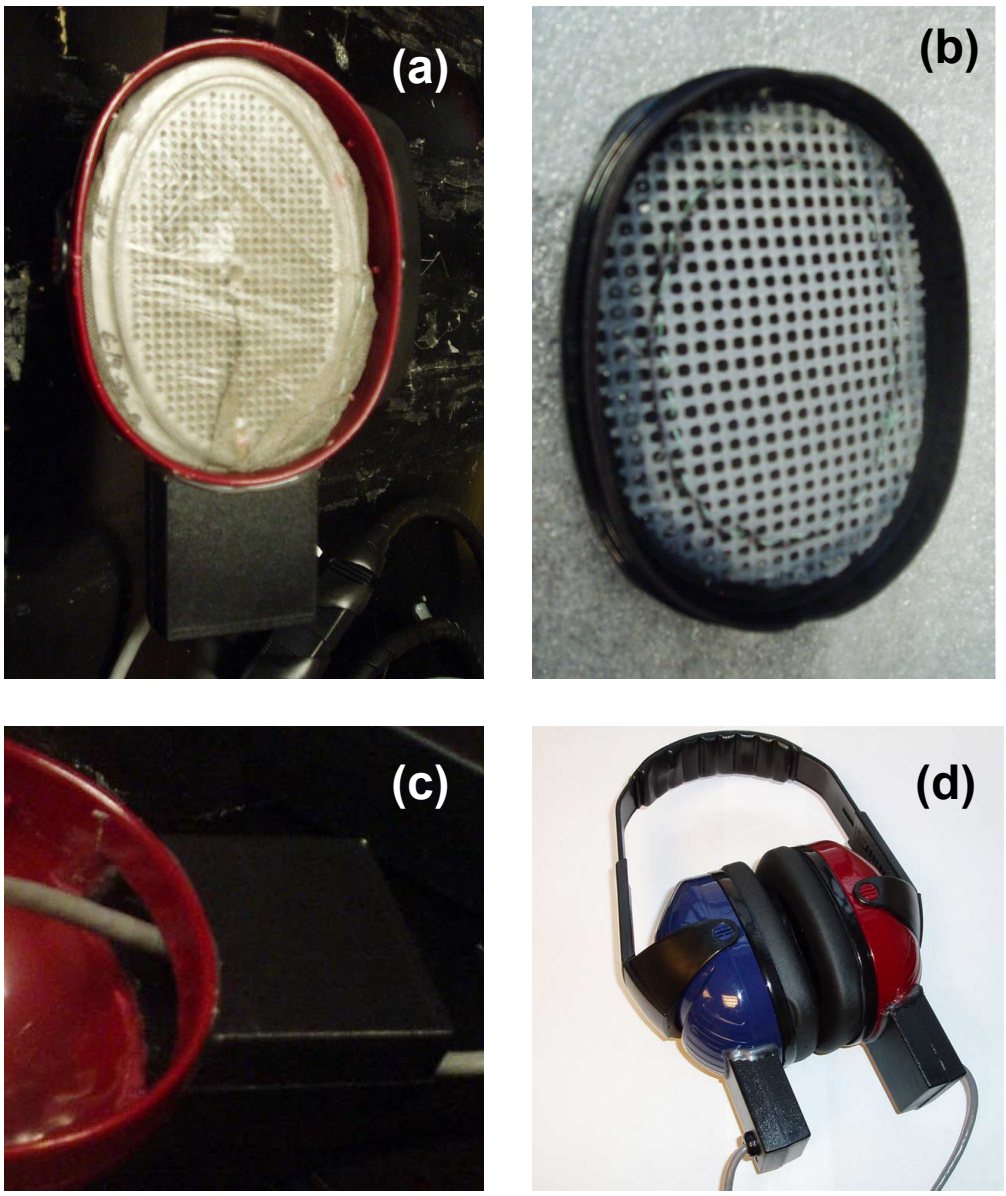

Figure 3A.6.1. Sound-attenuating headphone enclosures: (a) Internal view with electrostatic headphone elements in place; (b) Plastic grille secured within ear cushion; (c) Detail of aperture and box for headphone element connectors; (d) External view of enclosures fully assembled.

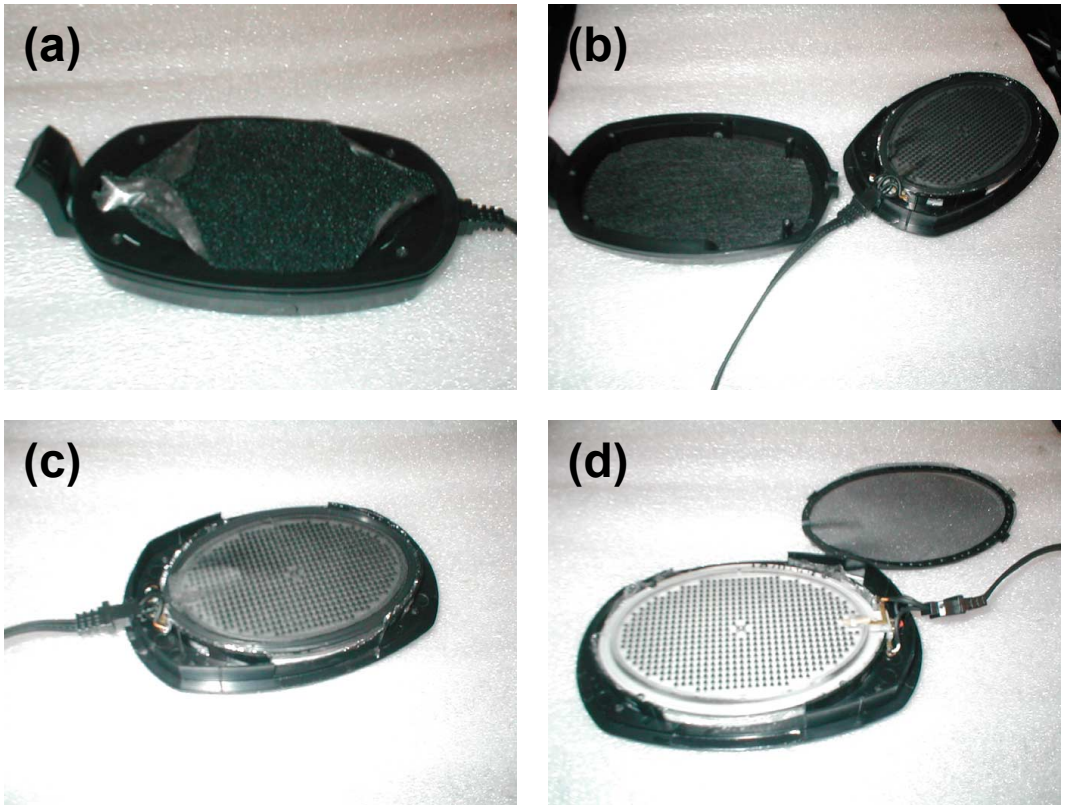

Figure 3A.6.2. Extraction of electrostatic elements from Koss ESP-950 headphones: (a) Exposure and removal of enclosure screws; (b) Separation of enclosure halves; (c) Retainer ring and protective mesh; (d) Removal of retainer ring and protective mesh, revealing electrostatic element, which can be snapped out of enclosure.

Connector Numbering (facing pin connector):

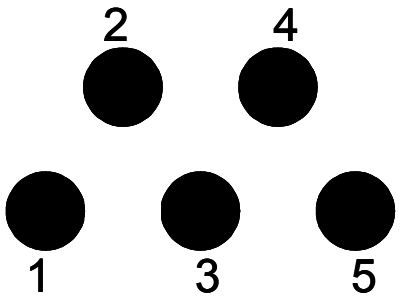

Pin #	Cable Color	Connection
1	Red	Right Inner Plate
2	Green	Right Outer Plate
3	Orange	Center Plate (R and L)
4	Yellow	Left Outer Plate
5	White	Left Inner Plate

("Inner" = closest to ear, "outer" = farthest from ear)

Figure 3A.6.3. Wiring chart for re-connecting electrostatic headphone elements. Wire colors refer to colors of inner insulators of original Koss cabling.

Figure 3A.6.4. Junction box showing shielded cable strain relief with Heyco connectors and spiral wrap cable protection.

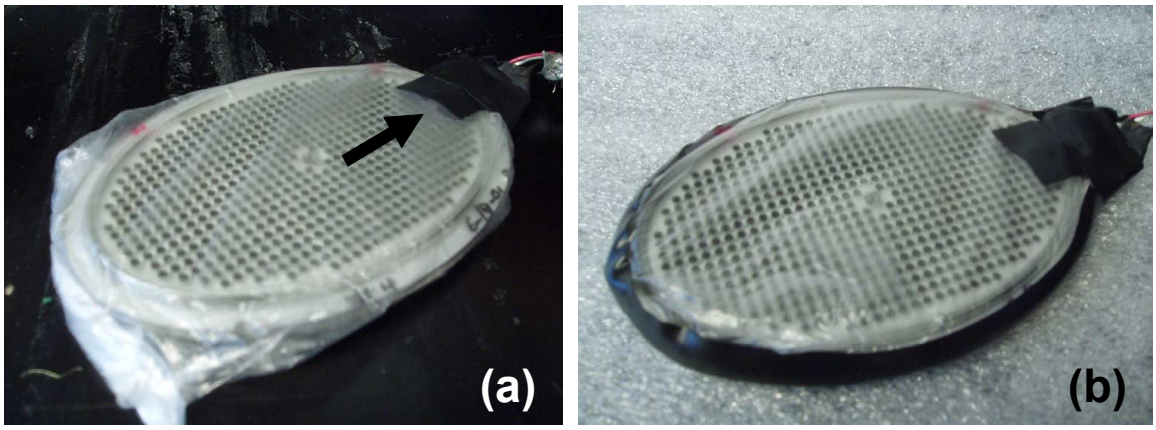

Figure 3A.6.5. Insulation for electrostatic headphone elements: Electrical connectors are protected by large-diameter shrink tubing (not shown); (a) Electrostatic element is sealed within thin single-layer plastic insulation and electrical tape is placed over conductors not covered by shrink tubing, illustrated by the arrow; (b) Edges of plastic insulation reinforced with electrical tape to protect against abrasion within headphone enclosure.

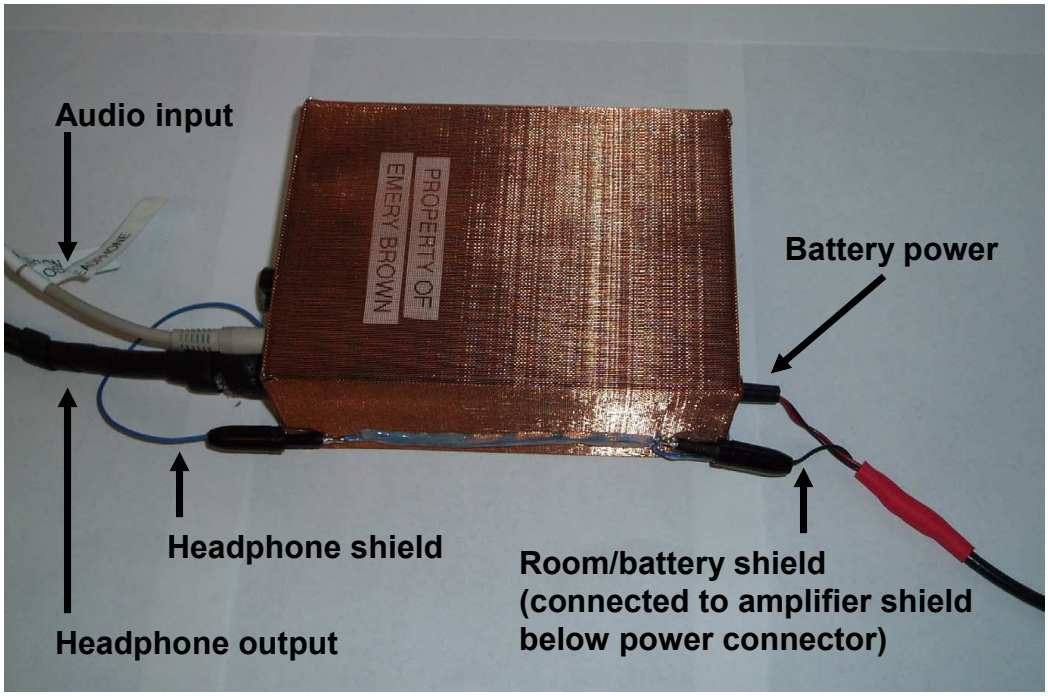

Figure 3A.6.6. Shield, ground, power, and audio inputs for modified Koss amplifier system.

Reference List

1. Angelone, L. M. and Bonmassar, G. Use of resistances and resistive leads: Implications on computed electric field and SAR values. Proc.12th ISMRM , 1652. 2004.
Ref Type: Abstract

2. Bishop RH (2001) Learning With Labview 6i. Upper Saddle River: Prentice Hall.

3. Bonmassar G, Anami K, Ives J, Belliveau JW (1999) Visual evoked potential (VEP) measured by simultaneous 64-channel EEG and 3T fMRI. Neuroreport 10: 1893-1897.

4. Burr-Brown Products. ADS1254: 24-bit, 20kHz, low power analog-to-digital converter. SBAS213. 2001. Dallas, TX, Texas Instruments, Inc.
Ref Type: Report

5. Garreffa G, Bianciardi M, Hagberg GE, Macaluso E, Marciani MG, Maraviglia B, Abbafati M, Carni M, Bruni I, Bianchi L (2004) Simultaneous EEG-fMRI acquisition: how far is it from being a standardized technique? Magn Reson Imaging 22: 1445-1455.

6. Goldman RI, Stern JM, Engel J, Jr., Cohen MS (2000) Acquiring simultaneous EEG and functional MRI. Clin Neurophysiol 111: 1974-1980.

7. Ives JR, Warach S, Schmitt F, Edelman RR, Schomer DL (1993) Monitoring the patient's EEG during echo planar MRI. Electroencephalogr Clin Neurophysiol 87: 417-420.

8. Lemieux L, Allen PJ, Franconi F, Symms MR, Fish DR (1997) Recording of EEG during fMRI experiments: patient safety. Magn Reson Med 38: 943-952.

9. Liebenthal E, Ellingson ML, Spanaki MV, Prieto TE, Ropella KM, Binder JR (2003) Simultaneous ERP and fMRI of the auditory cortex in a passive oddball paradigm. Neuroimage 19: 1395-1404.

10. Linear Technology Corporation. LT1167: Single resistor gain programmable, precision instrumentation amplifier. 1167fa LT/TP 0301 2K REV A. 1998. Milpitas, CA, Linear Technology Corporation.
Ref Type: Report

11. Mirsattari SM, Ives JR, Bihari F, Leung LS, Menon RS, Bartha R (2005) Real-time display of artifact-free electroencephalography during functional magnetic resonance imaging and magnetic resonance spectroscopy in an animal model of epilepsy. Magn Reson Med 53: 456-464.

12. Percival DB, Walden AT (1993) Spectral analysis for physical applications. New York: Cambridge University Press.

13. Vanni S, Dojat M, Warnking J, Delon-Martin C, Segebarth C, Bullier J (2004) Timing of interactions across the visual field in the human cortex. Neuroimage 21: 818-828.

14. Vasios, C. E., Angelone, L. M., Purdon, P., Belliveau, J. W., and Bonmassar, G. EEG measurements at 7T Tesla using the ink cap. 13th ISMRM (submitted) . 2005.
Ref Type: Abstract